2020

Northward Migration of the Oregon forearc on the Gales Creek fault

Ray E. Wells
Portland State University, rwells@pdx.edu

Richard J. Blakely
U.S. Geological Survey

Sean Bemis
Virginia Tech

Citation Details

Wells, R. E., Blakely, R. J., & Bemis, S. (2020). Northward migration of the Oregon forearc on the Gales Creek fault. Geosphere, 16(2), 660-684.

Research Paper

GEOSPHERE

GEOSPHERE, v. 16, no. 2

https://doi.org/10.1130/GES02177.1

16 figures; 2 tables; 3 high-resolution figure files

CORRESPONDENCE: rwells@usgs.gov

CITATION: Wells, R.E., Blakely, R.J., and Bemis, S., 2020, Northward migration of the Oregon forearc on the Gales Creek fault: Geosphere, v. 16, no. 2, p. 660–684, https://doi.org/10.1130/GES02177.1.

Science Editor: Shanaka de Silva
Associate Editor: Colin Amos

Received 12 July 2019
Revision received 30 October 2019
Accepted 6 January 2020

Published online 6 February 2020

Northward migration of the Oregon forearc on the Gales Creek fault

Ray E. Wells[1], Richard J. Blakely[2,*], and Sean Bemis[3]

[1]U.S. Geological Survey, 2130 SW 5th Street, Portland, Oregon 97201, USA
[2]U.S. Geological Survey, 345 Middlefield Road, MS 973 Menlo Park, California 94025, USA
[3]Global Forum on Urban and Regional Resilience, Virginia Tech, Blacksburg, Virginia 24061, USA

ABSTRACT

The Gales Creek fault (GCF) is a 60-km-long, northwest-striking dextral fault system (west of Portland, Oregon) that accommodates northward motion and uplift of the Oregon Coast Range. New geologic mapping and geophysical models confirm inferred offsets from earlier geophysical surveys and document ~12 km of right-lateral offset of a basement high in Eocene Siletz River Volcanics since ca. 35 Ma and ~8.8 km of right-lateral separation of Miocene Columbia River Basalt at Newberg, Oregon, since 15 Ma (~0.62 ± 0.12 mm/yr, average long-term rate). Relative uplift of Eocene Coast Range basalt basement west of the fault zone is at least 5 km based on depth to basement under the Tualatin Basin from a recent inversion of gravity data. West of the city of Forest Grove, the fault consists of two subparallel strands ~7 km apart. The westernmost, Parsons Creek strand, forms a linear valley southward to Henry Hagg Lake, where it continues southward to Newberg as a series of en echelon strands forming both extensional and compressive step-overs. Compressive step-overs in the GCF occur at intersections with ESE-striking sinistral faults crossing the Coast Range, suggesting the GCF is the eastern boundary of an R′ Riedel shear domain that could accommodate up to half of the ~45° of post–40 Ma clockwise rotation of the Coast Range documented by paleomagnetic studies. Gravity and magnetic anomalies suggest the western strands of the GCF extend southward beneath Newberg into the Northern Willamette Valley, where colinear magnetic anomalies have been correlated with the Mount Angel fault, the proposed source of the 1993 M 5.7 Scotts Mills earthquake. The potential-field data and water-well data also indicate the eastern, Gales Creek strand of the fault may link to the NNW-striking Canby fault through the E-W Beaverton fault to form a 30-km-wide compressive step-over along the south side of the Tualatin Basin. LiDAR data reveal right-lateral stream offsets of as much as 1.5 km, shutter ridges, and other youthful geomorphic features for 60 km along the geophysical and geologic trace of the GCF north of Newberg, Oregon. Paleoseismic trenches document Eocene bedrock thrust over 250 ka surficial deposits along a reverse splay of the fault system near Yamhill, Oregon, and Holocene motion has been recently documented on the GCF along Scoggins Creek and Parsons Creek. The GCF could produce earthquakes in excess of Mw 7, if the entire 60 km segment ruptured in one earthquake. The apparent subsurface links of the GCF to other faults in the Northern Willamette Valley suggest that other faults in the system may also be active.

*Current address: P.O. Box 158, 350 N. Akron Rd., Moffett Field, California 94035, USA

INTRODUCTION

The Juan de Fuca plate subducts obliquely to the northeast at ~40 mm/yr beneath the Northwestern United States and adjacent Canada along the Cascadia subduction zone (Wilson, 1993) (Fig. 1A). The oblique component of convergence reflects northward motion of the Pacific plate with respect to North America, and the resulting dextral shear couple along the margin drives clockwise rotation and northward migration of crustal blocks in the overlying North American plate (e.g., Beck, 1976, 1980; Magill et al., 1982; Grommé et al., 1986; Walcott, 1993; Pezzopane and Weldon, 1993; Wells et al., 1998; McCaffrey et al., 2007, 2013). Global Positioning System (GPS) data indicate that clockwise rotation and northward motion of the upper plate at ~8–12 mm/yr with respect to stable North America are occurring today (Fig. 1B; McCaffrey et al., 2007, 2013), and the resultant upper-plate faulting is a significant seismic hazard in the urban corridor of Oregon and Washington.

Large-scale strike-slip faulting and trench-parallel migration of the forearc commonly accompany oblique subduction (Fitch, 1972; Wang, 1996). In Cascadia, paleomagnetic and geodetic clockwise rotation rates increase toward the coast (Fig. 1C, Sheriff, 1984; England and Wells, 1991; McCaffrey et al., 2007, 2013), indicating permanent, margin-parallel, right-lateral shear in the forearc. Earthquake focal mechanisms and northwest alignments of seismicity in the Mount St. Helens seismic zone further suggest right-lateral motion on strike-slip faults is occurring in the Cascadia forearc (Weaver and Smith, 1983; Brocher et al., 2017). Although active thrust faulting is well documented in the Puget Lowland (e.g., Nelson et al., 2003; see Barnett et al., 2010, for an atlas of active structures), large-offset, right-lateral faulting has not been documented in the Oregon forearc.

In this work, we present a study of a set of en echelon, northwest-striking faults in the greater Portland, Oregon, metropolitan area to determine the history, sense of displacement, and potential for active faulting (Fig. 2). The Portland Hills, Sylvan-Oatfield, Canby, and Gales Creek faults are in the U.S. Geological Survey (USGS) Quaternary fault and fold database (USGS, 2010), but their location, sense of motion, and slip rates are not well understood. Beeson et al. (1989a) suggested these faults were primarily right-lateral based on their linear, northwest trend, and they proposed that they formed pull-apart basins that promoted basaltic volcanism of the Pliocene and Quaternary Boring volcanic field in and around Portland.

Aeromagnetic and gravity surveys of NW Oregon reveal one of these northwest faults, the Gales Creek fault (GCF), to be the major structure in the northwest Oregon forearc. Blakely et al. (1995, 2000) showed the GCF to be the

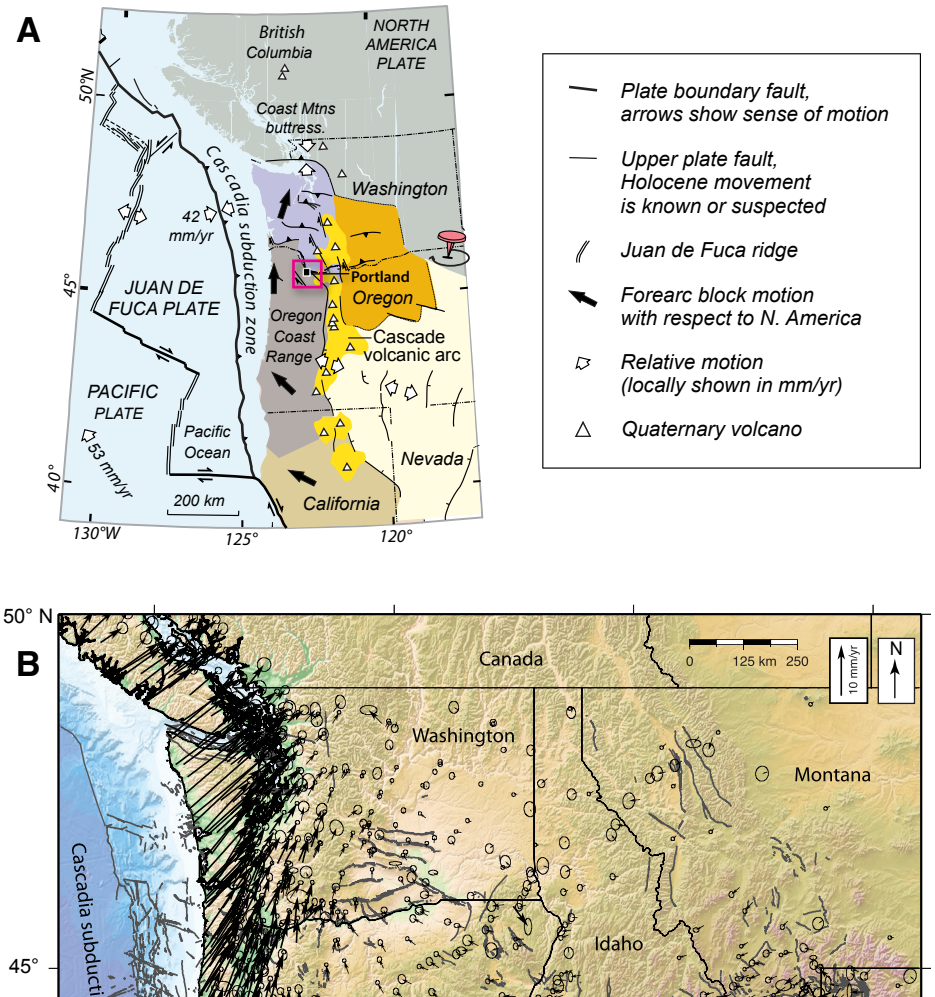

Figure 1. (A) Tectonic setting of the Cascadia convergent margin. Oregon Coast Range block (dark brown) rotating about a pole in the backarc (schematically illustrated by thumbtack) is migrating north at ~8 mm/yr near Portland (modified from Sherrod et al., 2004). California's Sierra Nevada—tan; Washington forearc deformation zone—purple; and Yakima Fold Belt—orange; red box shows area of Figure 2. (B) Clockwise rotation and northward motion of the forearc from the GPS velocity field (modified from McCaffrey et al., 2016). (C) Clockwise paleomagnetic (Pmag) rotations and geodetic (GPS) rotation rates increase toward the coast (in degrees). In E-W profile, at bottom, paleomagnetic rotation rates for 12 and 15 Ma Pomona and Ginkgo flows of the Columbia River Basalt Group are similar to GPS rotation rates, indicating rotation is converted to permanent deformation, consistent with westward increasing dextral shear along the margin (modified from Wells and McCaffrey, 2013).

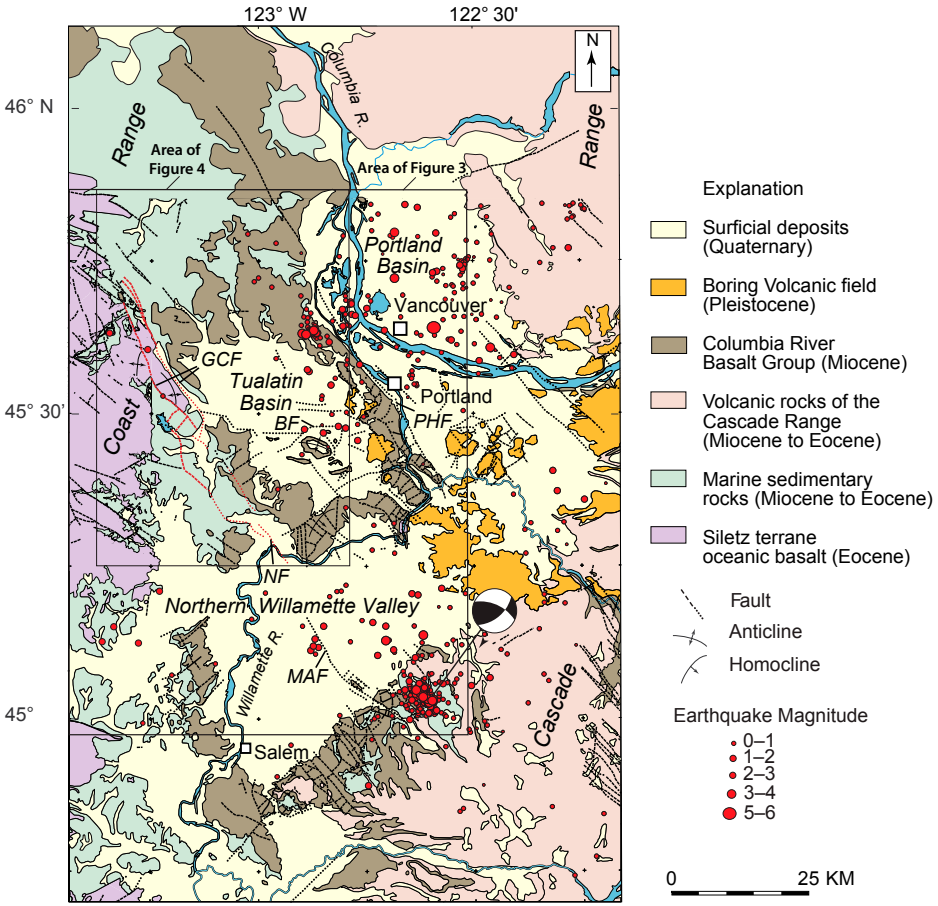

Figure 2. Regional geologic map of the Portland-Salem, Oregon area showing crustal seismicity, 1993 Scotts Mills earthquake focal mechanism, and area of Figures 3 and 4 (modified from Blakely et al., 2000). Abbreviations: PHF—Portland Hills fault; BF—Beaverton fault; GCF—Gales Creek fault (red lines); MAF—Mount Angel fault; NF—Newberg fault.

largest of a series of northwest-trending, linear aeromagnetic anomalies that coincided with mapped faults, including the Canby fault and the Sylvan-Oatfield fault in the Tualatin Mountains near Portland (Fig. 3A). They proposed that the Canby fault and the GCF were right-lateral faults based on apparent offset of Eocene basement magnetic anomalies, and that magnetic anomalies may link the GCF to the Mount Angel fault (MAF), as suggested by Beeson et al. (1989a). McPhee et al. (2014) inverted gravity data (Fig. 3B) to determine that the GCF and Portland Hills faults (PHF) form the boundaries of a pull-apart basin in Siletz River Volcanics basement, which is 5 km deep beneath the Tualatin Valley.

We combined new geologic mapping, high-resolution topographic data (also known as light detection and ranging [LiDAR]), trenching, and selected magnetic profiles along with the aeromagnetic and gravity surveys to examine the structure and geologic history of the GCF, which locally forms the boundary between the northern Coast Range and the Willamette Valley (Schlicker and Deacon, 1967; Blakely et al., 2000; McPhee et al., 2014; Wells et al., 2018, 2019). Geologic mapping of the GCF was part of a larger mapping effort to determine the tectonic setting and potential for active faulting in the greater Portland-Vancouver-Hillsboro metropolitan area and surrounding regions of Oregon and Washington (Wells et al., 2018, 2019). Mapping at 1:24,000 scale on U.S. Geological Survey (USGS) 7.5′ quadrangle maps was done intermittently in 1996–1997 and 2001–2007, and it was remapped on LiDAR topography and field checked in 2009–2010. Our work shows that the GCF is a major crustal structure that extends northwest from Newberg, Oregon, at least 60 km north to the Nehalem River. In this paper, we document ~12 km of northward motion of the Coast Range on the GCF since the Eocene, and we present paleoseismic evidence for Quaternary activity on the fault.

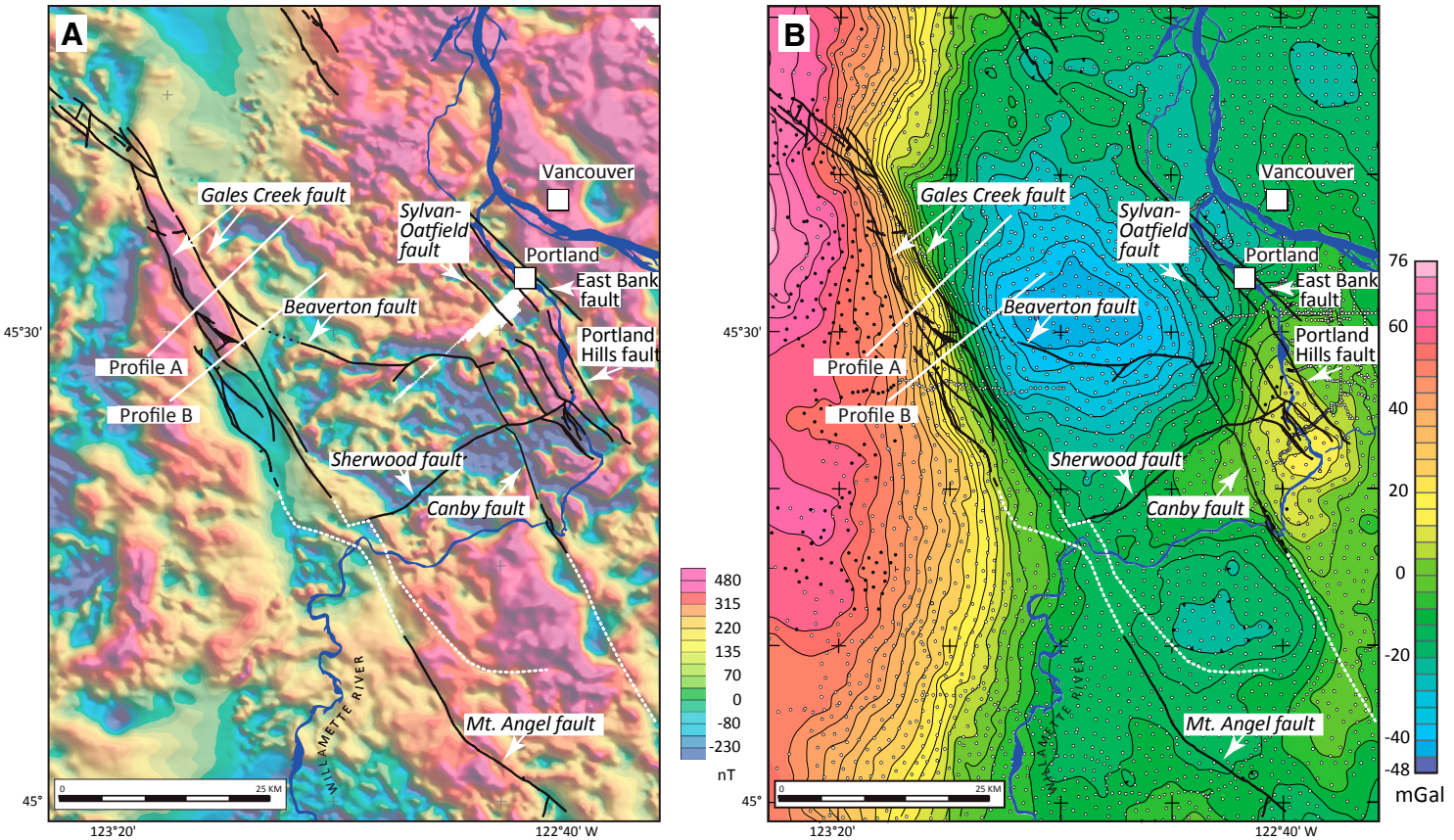

Figure 3. Large potential-field gradients across the Gales Creek fault (GCF) and related structures, northwest Oregon. (A) Aeromagnetic anomaly map (modified from Blakely et al., 2000), scale in nanoteslas (nT). (B) Isostatic gravity anomaly map (modified from McPhee et al., 2014), scale in milliGals. Simplified faults are from McPhee et al. (2014). White dotted lines indicate suggested links between GCF and Mount Angel and Canby faults (modified from Blakely et al., 2000). Solid white lines are locations of crustal models in Figure 6.

STRUCTURE OF THE GALES CREEK FAULT

In northwest Oregon, the Gales Creek fault (GCF) forms the eastern boundary of the Coast Range uplift, a broad, north-plunging anticlinorium exposing Paleogene oceanic basaltic basement of the Siletz River Volcanics (SRV, also known as the Siletzia terrane) in its core (Snavely et al., 1968; Wells et al., 2014). The GCF juxtaposes rocks of the Siletzia terrane against overlying marine and continental strata of the Tualatin Basin to the east (Fig. 2). Schlicker and Deacon (1967) originally mapped the GCF in the northwest-trending valley of Gales Creek, with short, en echelon faults stepping south to Carpenter Creek and the Chehalem Valley, and Yeats et al. (1996) proposed that a short, northwest-striking fault underlies Newberg (see Fig. 4A for local geographic names). Beeson et al. (1989a) speculated that the GCF extends southeast into the Northern Willamette Basin, where it has been interpreted to link to the northwest-striking Mount Angel fault (MAF), the inferred source of the 1993 M 5.7 Scotts Mills earthquake (Fig. 2). Blakely et al. (2000) interpreted aeromagnetic anomalies in the Northern Willamette Basin to be consistent with this idea, and that restraining bends in the faults suggested by the anomalies were consistent with the oblique right-lateral thrust focal mechanism of the earthquake (Thomas et al., 1996; Figs. 2 and 3A). Southeast of Mount Angel, the MAF heads into the western Cascades, where its extent is unknown. To the north, the central GCF segment appears to be truncated at a series of

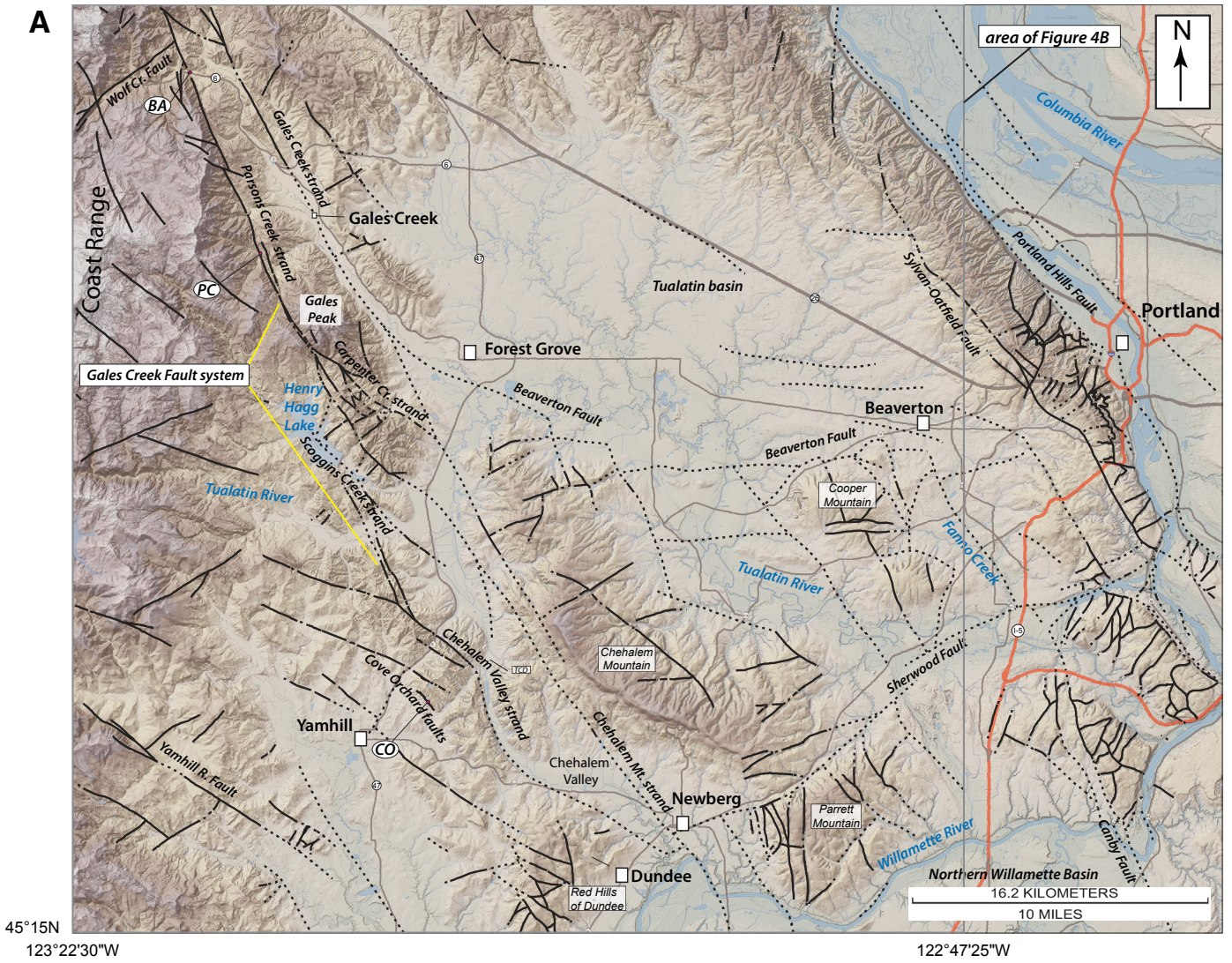

Figure 4. (A) Physiographic map of the Gales Creek fault (GCF) and surrounding area showing features named in text, light detection and ranging (LiDAR) topography from the Oregon Lidar Consortium. (*Continued on following page.*)

B

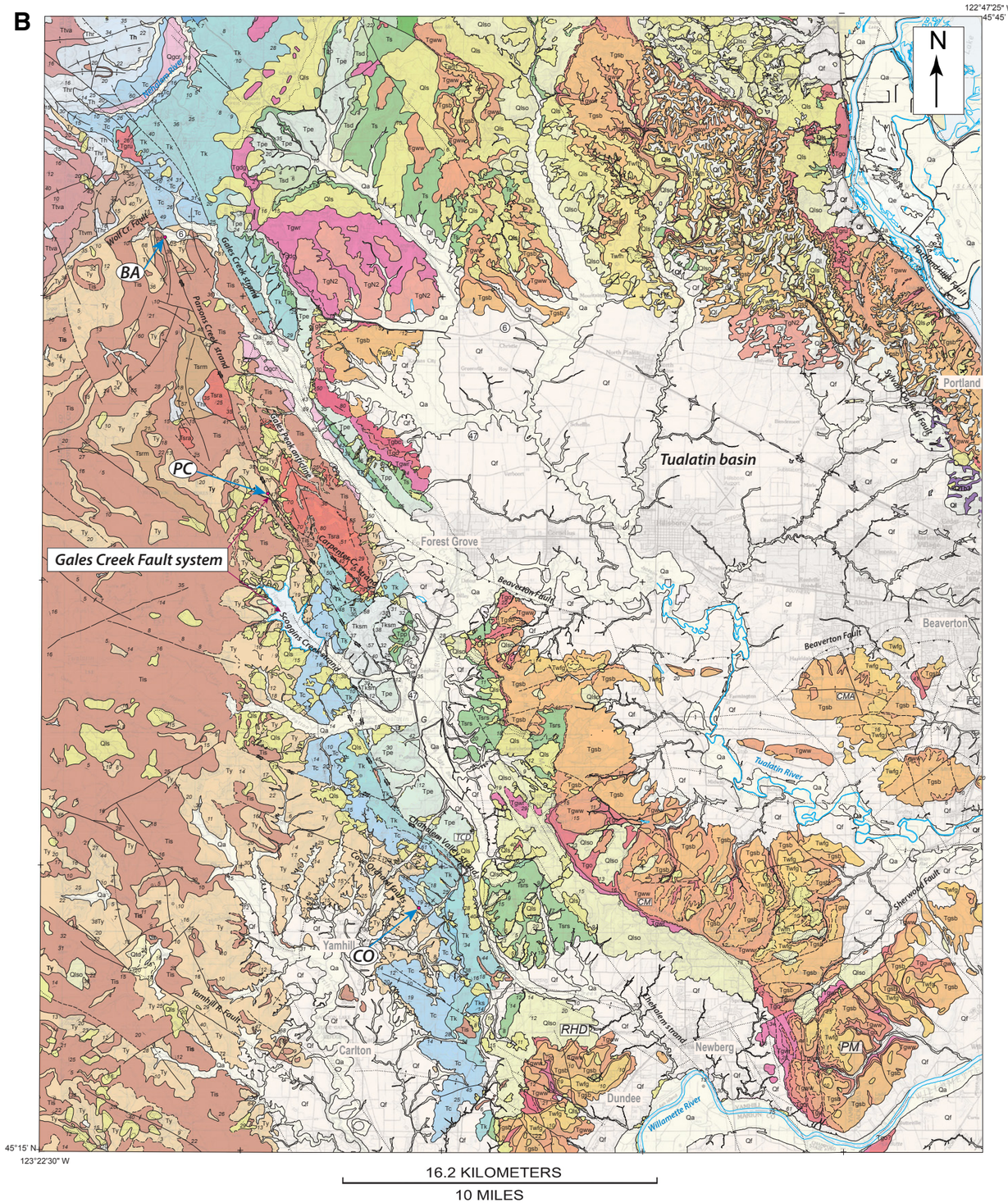

LIST OF MAP UNITS

UNCONSOLIDATED DEPOSITS

- af — Artificial fill (Holocene)
- Qa — Alluvium (Holocene)
- Qe — Eolian deposits (Holocene)
- Qls — Landslide deposits (Holocene and Pleistocene)
- Qlso — Older landslide deposits (Pleistocene)
- Qaf — Alluvial fan deposits (Pleistocene)
- Ql — Loess (Holocene and Pleistocene)
- Qtd — Terrace deposits (Holocene and Pleistocene)
- Qf — Missoula Flood deposits (Pleistocene)
- Qfc — Coarse-grained Missoula Flood deposits (Pleistocene)

BASIN FILL

- Qgcr — Gravel of Coast Range origin (Pleistocene)
- QTcr — Older gravel of Columbia River origin (Pleistocene and Pliocene)
- QTb3 — Rocks of the Boring volcanic field (Pleistocene and Pliocene)
  1.4–1.7 Ma basalt flows

COLUMBIA RIVER BASALT GROUP

Wanapum Basalt (Miocene)
Frenchman Springs Member

- Twfh — Basalt of Sand Hollow
- Twfg — Basalt of Ginkgo

Grande Ronde Basalt (Miocene)

- TgN2 — N2 flows, undivided
- Tgsb — Sentinel Bluffs Member
- Tgww — Winter Water member
- Tgu — Umtanum member
- Tgo — Ortley member
- Tgbc — Buttermilk Canyon member
- Tgac — Armstrong Canyon member
- Tgru — N2 and R2 flows, undivided
- TgR2 — R2 flows, undivided
- Tggc — Grouse Creek member
- Tgwr — Wapshilla Ridge member

N1 flows

- Tgdg — Downey Gulch member

INTRUSIVE ROCKS

- Tis — Intrusive rocks of the Coast Range (Eocene)

VOLCANIC AND SEDIMENTARY ROCKS OF THE COAST RANGE

- Ts — Scappoose Formation, undivided (Miocene and Oligocene)—Sandstone, divided into:
- Tsrs — Ribbon Ridge member (Oligocene)
- Tsrt — Tuffaceous mudstone (Oligocene)
- Tsd — Divide member (Oligocene)
- Tpb — Pittsburg Bluff Formation (Oligocene and Eocene)—Sandstone and mudstone, divided into:
- Tpe — East Fork member (Oligocene and Eocene)
- Tpp — Pebble Creek member (Eocene)
- Tk — Keasey Formation, undivided (Eocene)—Mudstone and sandstone, divided into:
- Tksm — Stimson Mill member
  Basaltic sandstone, contains:
- Tkst — Tuff bed
- Tks — Sandstone
- Tc — Cowlitz Formation (Eocene)—Sandstone, includes the Spencer Formation
- Th — Hamlet formation (Eocene)—Mudstone and sandstone, divided into:
- Thr — Roy Creek member
  Basaltic sandstone
- Tillamook Volcanics (Eocene)—Basalt, divided into:
- Ttva — Subaerial flows
- Ttvm — Submarine flows and breccias
- Ty — Yamhill Formation (Eocene)
- Siletz River Volcanics (Eocene)—Basalt, divided into:
- Tsra — Subaerial flows
- Tsrf — Mudstone interbeds
- Tsrm — Submarine flows and breccias

Contact—Solid where location is certain; dashed where location is approximate; dotted where location is concealed. Queried where uncertain

Fault—Solid where location is certain; dashed where location is approximate; dotted where location is concealed. Queried where uncertain

Figure 4 (*Continued*). (B) Geologic map of the Gales Creek fault and surrounding area, modified from Wells et al. (2019). Selected features labeled: RHD—Red Hills of Dundee; PM—Parrett Mountain; CM—Chehalem Mountain; BA—Bloggett Arboretum trench site; PC—Parsons Creek trench site (Parsons Creek in blue); CO—Willakenzie vineyard trench site; TCD—Tualatin-Chehalem divide.

west-trending faults cutting across the Coast Range toward the coast (Niem and Niem, 1985; Wells et al., 1995).

The main focus of this paper is the 60-km-long central segment of this system, the GCF sensu stricto, from Newberg northward through Henry Hagg Lake reservoir to just west of Timber, on the Nehalem River (Figs. 4A and 4B). Field work in the segment west of the Tualatin Basin shows the fault to consist of two strands, one in Gales Creek and another 7 km to the west in the valley of Parsons Creek (Wells et al., 2018, 2019). The two strands are quite linear, striking ~340°, and they bound the north-plunging Gales Peak anticline, which is cored by subaerial basalt flows and interbedded sediments of the Siletz River Volcanics, dated at 49 Ma (Wells et al., 2014). The pop-up anticline suggests the faults may have a reverse component, consistent with the 5 km vertical offset of Siletzia basement inferred from the gravity inversion (McPhee et al., 2014). The Gales Creek strand lies within the broad Gales Creek Valley and has limited geomorphic expression. It is mapped on the basis of northwest-striking, vertical shear zones and near-vertical, northwest-striking bedding of the Eocene Keasey Formation exposed intermittently along the Gales Creek streambed northwest of Forest Grove (Figs. 4A and 4B). Along the Gales Creek strand, the Grande Ronde Basalt of the Columbia River Basalt Group (16 Ma) dips 25°–30° to the northeast, into the Tualatin Basin, away from the fault. The Parsons Creek strand west of Gales Creek follows a series of aligned, narrow, linear valleys to the northwest, where it crosses and offsets Gales Creek at the State Route 6 bridge over the creek (Fig. 4A). North of Highway 6, the fault is truncated by the WNW faults that bound the north side of the uplifted Tillamook Volcanics block (Niem and Niem, 1985; Wells et al., 1995, Fig. 4B).

At Henry Hagg Lake, the Parsons Creek strand splays into several strands and steps south into the Scoggins Creek drainage through a series of short, northeast-striking linking faults (Fig. 4A). The main strand in Scoggins Creek crosses a saddle in the Scoggins-Tualatin River divide, where a Bureau of Reclamation trench exposed a sliver of basaltic sandstone faulted into the tuffaceous Eocene Keasey Formation within a 30-m-wide zone of high-angle, strike-slip faults (Redwine et al., 2017). South of the Scoggins-Tualatin divide, the Scoggins Creek and Chehalem Valley strands form two pronounced restraining bends at the Chehalem-Tualatin divide and around the Red Hills of Dundee (Fig. 4A).

The restraining bends mark intersections with N70°W sinistral faults that cross the Coast Range (Wells et al., 1995) and apparently offset the GCF (Fig. 4B). Two other splays of the Parsons Creek strand, the Carpenter Creek and Chehalem Mountain strands, are thought to cross Highway 47, where industry seismic lines reveal faulted Cenozoic strata (Jack Meyer, 2001, 2018, written commun.) and head SSE beneath the landslide complex on the west side of Chehalem Mountain. At Newberg, all strands of the GCF apparently step left around the Red Hills of Dundee and pass through the broad Newberg low at the south end of Chehalem Creek, beneath Missoula flood deposits and alluvium.

Two major NE-trending faults intersect the GCF and are truncated by it—the Sherwood fault extending from Lake Oswego to Newberg and the Wolf Creek fault near Highway 6 (Figs. 4A and 4B). These faults have large vertical offset (0.3–1 km) from their map relations but are typically offset by the younger NW-trending faults. The Sherwood fault is down to the north and may be a thrust or reverse fault. The Wolf Creek fault is also down to the north, dropping Tillamook Volcanics down against SRV in the south block (Fig. 4B and Wells et al., 1995). Both faults may represent reactivation of old basement structures in the Siletz terrane related to its accretion (Wells et al., 2014).

GEOPHYSICAL SIGNATURE

The GCF is the largest crustal fault in NW Oregon, based on gravity and aeromagnetic surveys that highlight structures in the dense, magnetic, basaltic forearc basement of the Siletz terrane (Blakely et al., 2000; McPhee et al., 2014). Potential-field data define a 110-km-long, linear feature along the GCF and the eastern margin of the Coast Range that extends southeastward beyond the mapped trace of the fault toward the Mount Angel fault in the Northern Willamette Basin (Fig. 3). These potential-field data suggest that the GCF is the western margin of a larger strike-slip fault system that includes the Mount Angel fault to the south and the Portland Hills–Canby fault system to the east, as suggested by Beeson et al. (1989a), Blakely et al. (2000), and McPhee et al. (2014).

Gravity

The USGS collected data from 3000 gravity stations in the greater Portland metropolitan area to better define the structure of the basins and their bounding faults (Morin, et al., 2007). The survey revealed a major gravity anomaly of up to 124 mGal across the GCF between the Coast Range and the Tualatin Basin. McPhee et al. (2014) inverted these gravity data to estimate the depth and shape of Siletz basement. Their inversion indicates that the Tualatin basement is 5 km deep and filled with low-density sediments that sharply contrast with high-density Siletz basement beneath the basin and along the GCF at Gales Peak (elevation 550 m). Their calculated basin fill is consistent with interpretations of seismic profiles and exploration wells (Yeats et al., 1996; Oregon Department of Geology and Mineral Industries, 2012) and our mapped thickness of Eocene to Miocene strata dipping eastward off the Coast Range into the basin (Fig. 4B; Wells et al., 2019; Oregon Department of Geology and Mineral Industries, 2012). This thick sedimentary section dipping into the basin indicates the basin began filling in the Eocene.

Aeromagnetic Data

Aeromagnetic surveys of the forearc (Fig. 3A) highlight the structure and stratigraphy of the basaltic Siletz basement, the overlying late Eocene Tillamook Volcanics, the Miocene Columbia River Basalt Group, and the Pleistocene flows of the Boring volcanic field, all of which contain both normal- and reverse-polarity magnetostratigraphic units in NW Oregon (Simpson and Cox, 1977;

Magill et al., 1981; Wells et al., 1989; Blakely et al., 2000; Fleck et al., 2014). Prominent negative anomalies correlate with reverse flows of Boring vents east of the map area (Fig. 4B); the Wapshilla Ridge Member of the R2 magnetozone of the Grande Ronde Basalt on the summit of Chehalem Mountain (Fig. 4A; CM, Fig. 4B); and reverse flows of the Tillamook Volcanics (Ttv, Fig. 4B) just north of 45°30′N along the western boundary of the map area. The striped pattern of magnetic highs and lows west of the GCF correlates with folded basalt flows and intrusions of Siletz River Volcanics, with strongly magnetic diabase (Tis) overlying less magnetic (or possibly reverse-polarity) pillow basalt (Tsrm, Fig. 4B).

Blakely et al. (2000) noted the aeromagnetic high over the Gales Peak anticline (Fig. 4B), which consists of subaerial basalt of the SRV and folded diabase, appears offset 10–12 km in a right-lateral sense across the GCF at Scoggins Dam (Figs. 3A and 5). McPhee et al. (2014) suggested the GCF and the PHF form the margins of a large Eocene pull-apart basin, based on the shape of the Tualatin Basin gravity anomaly. This model requires substantial right-lateral motion, possibly several kilometers, on the GCF in the Eocene. A set of WNW linear anomalies in the Coast Range coincide with WNW-striking faults that have sinistral offset of Paleogene strata and also offset the GCF. The numerous WNW-striking anomalies suggest that the sinistral faulting in

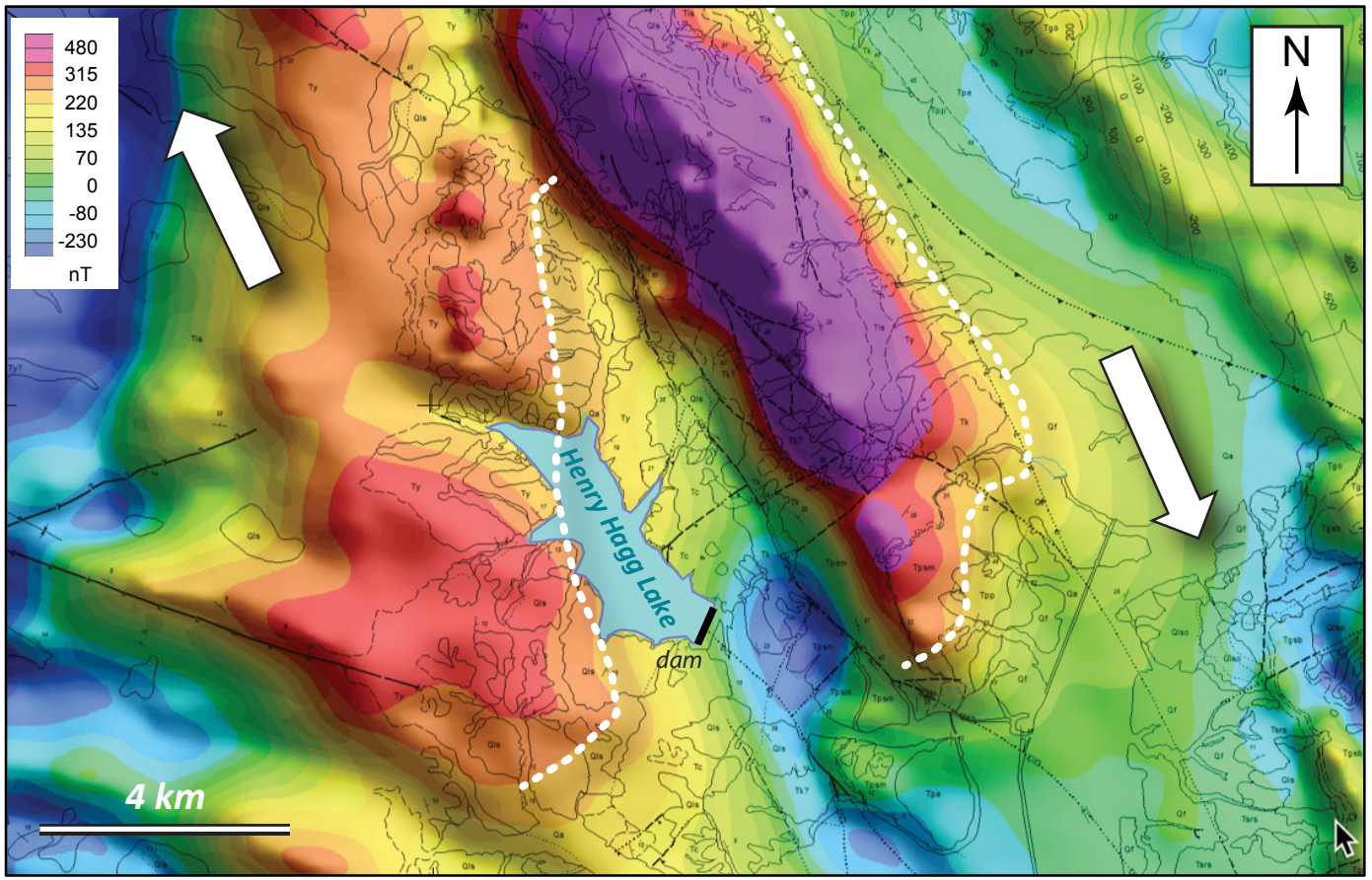

Figure 5. Apparent offset of magnetic Siletzia basalt basement, Henry Hagg Lake area, southwest of Forest Grove, Oregon. Separation of magnetic anomaly contour (white dots) is ~10 km in a right-lateral sense (white arrows). Geologic linework as in Figure 4.

the Coast Range may be widespread (compare Figs. 3A and 4B and see later discussion). Along the Canby fault, anomalies correlated with basement of Siletz River Volcanics appear to be offset right laterally a minimum of 5 km (Blakely et al., 2000).

Gravity and Magnetic Models of Fault Structure

We used measured gravity and magnetic anomalies to construct two geologic cross sections across the GCF to better understand subsurface structure (Figs. 3 and 6). The cross sections are based on gridded, ground-based gravity and airborne magnetic data and constrained by mapped geology, available seismic-reflection data, and other subsurface information. The models were constructed by forward (trial-and-error) modeling of crustal sources in order to simultaneously fit calculated gravity and magnetic anomalies to field observations. Modeled bodies were assumed to be two-dimensional in shape; i.e., infinitely extended in the directions perpendicular to the profiles. This assumption is appropriate for linear anomalies along the GCF but may introduce minor errors where anomalies are less linear. We further assumed that the direction of magnetization in each body is either parallel or antiparallel to Earth's magnetic field. This second assumption is appropriate for rocks dominated by induced magnetization and approximately correct for rocks with large remanent magnetizations. Density and magnetizations are consistent with published models from similar Cascadia geologic settings (e.g., Finn, 1990). It is important to recognize that our cross sections are not unique, a limitation of all potential-field modeling (Blakely, 1995). Although other models will fit the observed data equally well, the cross sections in Figure 6 are consistent with geologic and other geophysical evidence.

Profile A (Fig. 6A) extends northeast from exposures of Eocene intrusive rocks at its southwest end, over Gales Peak anticline and into the Tualatin Basin. Profile B (Fig. 6B) also strikes northeast and crosses the city of Forest Grove and the deepest part of the Tualatin Basin.

Both profiles illustrate an interesting aspect of gravity and magnetic fields in this region. The gravity field is characterized by a broad, relatively smooth anomaly, in contrast to high-amplitude, short-wavelength magnetic anomalies typical of Cascadia terrane. Part of this difference in anomaly character is due to differing theoretical properties of gravity and magnetic fields (Blakely, 1995), but in this region it also reflects the nature and depth of gravity versus magnetic sources. We hypothesize that the broad gravity anomaly is dominated by dense basaltic rocks of Siletzia, modeled at a depth of 3–6 km beneath the Tualatin Basin but uplifted to shallower depths in the Coast Range. The uplifted Siletzia basement reflects the eastern shoulder of the Coast Range anticlinorium farther to the west. Magnetic anomalies, on the other hand, are sensitive to near-surface (less than ~2-km-depth) contacts, such as juxtaposed normally and reversely magnetized bodies, faulted magnetic rocks, and sedimentary basins.

Both cross-sectional models exhibit steep faults with significant vertical offset, in accordance with the transpressive evolution of the GCF. Profile A (Fig. 6A) indicates an anticlinal pop-up, bounded on the west and east, respectively, by the Parsons Creek and Gales Creek strands of the GCF, consistent with geologic mapping (Fig. 4). The model indicates 1–2 km of vertical offset of Eocene rocks along the Parsons Creek and Gales Creek faults at this locale. Profile B (Fig. 6B) also indicates a pop-up structure, exposing at this locale weakly magnetic basaltic sandstone of the Late Eocene and Early Oligocene Stimson Mill member of the Keasey Formation. The reverse fault on the western side of the pop-up is interpreted as the Scoggins Creek strand of the GCF, which continues southeastward toward the Mount Angel fault (Figs. 4A and 4B). Profile B includes a buried, reversely magnetized dike swarm intruded along the Scoggins Creek fault, necessary to fit the short-wavelength, negative magnetic anomaly over Scoggins Creek. Similar intrusions are exposed along the GCF north and south of the profile, but no dike is exposed at the surface at profile B.

RIGHT-LATERAL OFFSET AND SLIP RATE

Offset Eocene Anticline

There are several lines of geologic evidence for right-lateral motion on the GCF (Fig. 7). The fold axis of the Gales Peak anticline that lies between the two fault strands curves westward into the Parsons Creek (western) strand of the GCF and is truncated by it (Fig. 7A). Another anticline cored by subaerial SRV lies west of the Parsons Creek strand and 12 km north of the Gales Peak anticline to the east. The western anticlinal axis curves eastward into the Parsons Creek strand and is truncated by it. Subaerial SRV is uncommon and localized around source vents in the Oregon Coast Range (Wells et al., 1995, 2000, 2014; Snavely et al., 1968, 1976; thus, we interpret the two anticlines as one anticline that has been sheared and faulted by the GCF. The anticline axis is offset dextrally 11 km if we use the local cut-off points of the axis, and 13.4 km if we project the broader anticlinal trends to the fault (adding the sharp bend in the axis adjacent to the fault to the displacement; Fig. 7). At the top of the SRV, the fold includes a regional diabase sill complex that provides a maximum age of the fold, as the diabase intrudes ~40-m.y.-old strata in Gales Creek and has a U/Pb age as young as 35 Ma about 15 km southwest of the study area (Wells et al., 2014). The observed offset of the folded Eocene volcanic rocks is nearly the same as the apparent offset (as shown in close-up in Fig. 5) observed in the associated magnetic anomalies. The mapped right-lateral offset matches the 10–12 km right-lateral offset determined by Blakely et al. (2000) based on displaced basement (Eocene) magnetic anomalies across the Parsons Creek strand of the GCF.

In addition to the offset anticline, Paleogene marine strata are strongly deformed where they cross the GCF. Northwest-striking Cowlitz sandstone, Keasey mudstone, and sandstone are rotated 45° clockwise between the Scoggins and Parsons Creek strands of the GCF (Fig. 7B). The marine strata in the fault zone typically are steeply dipping, and Z-folds plunging 45° northwest

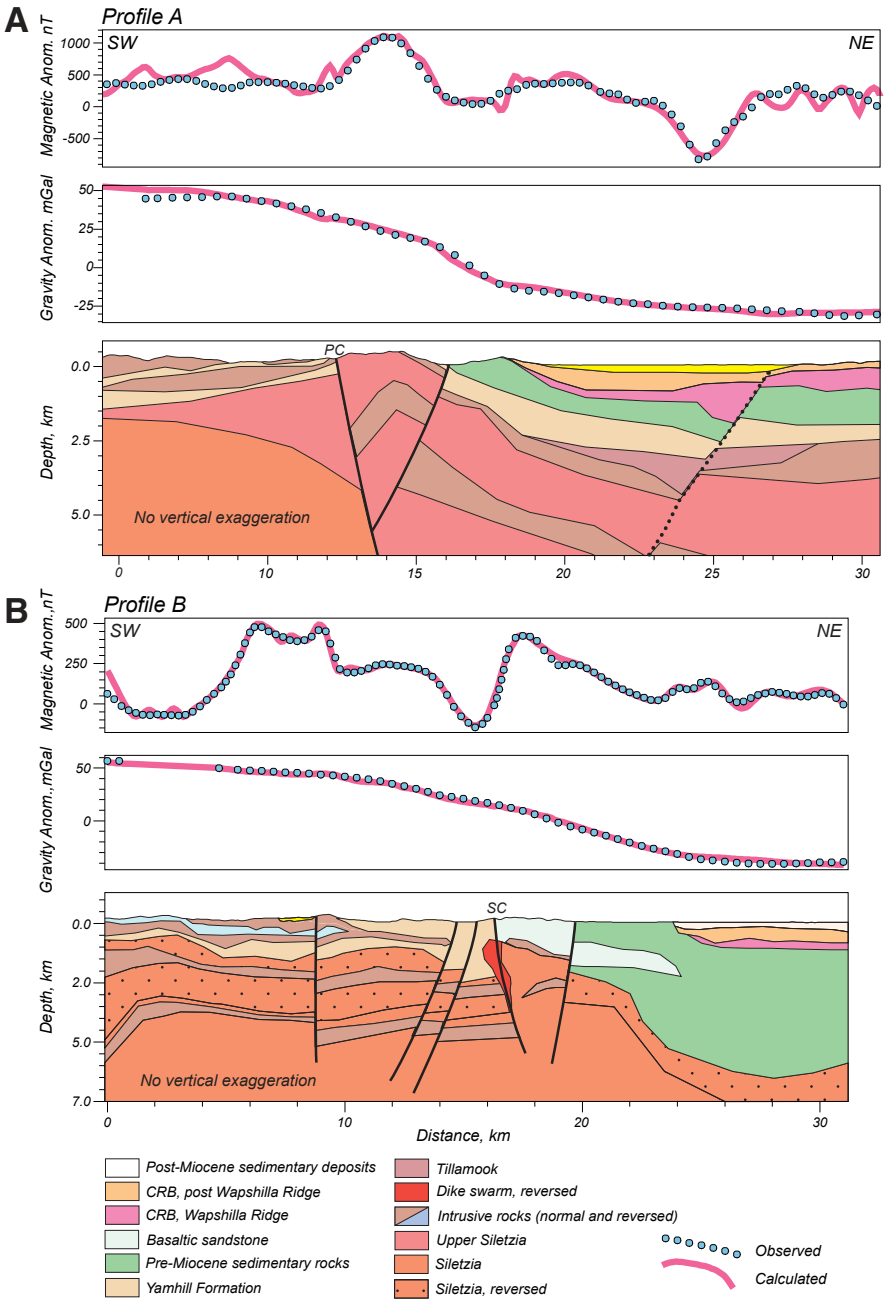

Figure 6. Cross-sectional models of the Gales Creek fault (GCF) determined from simultaneous forward modeling of gravity and airborne magnetic data. (A) Northeast-directed profile over Gales Peak, showing pop-up anticline facilitated by inferred reverse slip on the Parsons Creek (PC) and Gales Creek strands of the GCF. (B) Northeast-directed profile over Forest Grove, exhibiting a pop-up of weakly magnetic basaltic sandstone of the Eocene Stimson Mill member of the Keasey Formation. Reverse slip on the Scoggins Creek strand (SC) of the GCF facilitated formation of the pop-up. CRB—Columbia River Basalt.

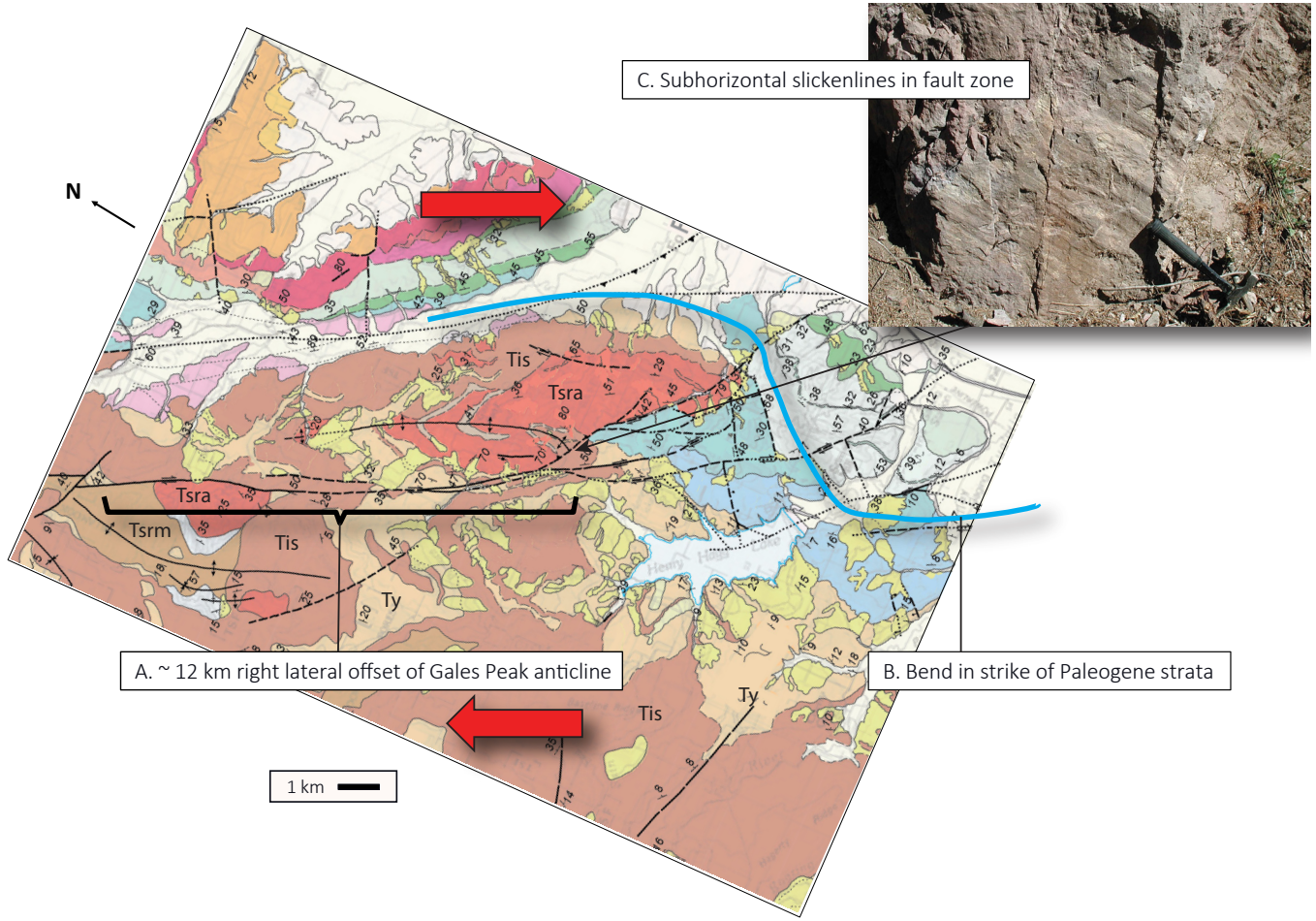

Figure 7. Geologic evidence for right-lateral motion on the Gales Creek fault (GCF). Map units as in Figure 4. (A) 12 km offset, bending, and truncation of Gales Peak anticline axis at GCF. Offset anticline is composed of folded subaerial Siletz River Volcanics (Tsra) and overlying diabase sills (Tis), which are strongly magnetic; see Figure 6. (B) Strike of Paleogene strata rotated clockwise into fault zone. (C) Subhorizontal slickenlines, view to NE.

(too small to show on map), consistent with dextral shear, occur in marine strata adjacent to the Parsons Creek strand. Subhorizontal slickenlines in faulted volcanic rocks are exposed in road cuts adjacent to the fault and in trenches across the fault (Fig. 7C; Redwine et al., 2017).

The 12.1 ± 1.1 km dextral offset of the Gales Peak anticline provides a minimum average dextral slip rate of 0.35 km/Ma for the Parsons Creek strand, if the anticline postdates folded sills as young as 35 Ma, or 0.76 km/Ma, if the fold largely postdates tilted 16 Ma flows of the CRBG.

Offset Margin of the Neogene Northern Willamette Basin

The Tualatin and Northern Willamette Basins are essentially Neogene "bathtubs" lined with far-traveled flows of the Columbia River Basalt Group and filled with post-CRBG sediment (Figs. 2 and 4B). The basins reflect continued subsidence (16 Ma CRBG is nearly 400 m below sea level, Wilson, 1997) and deformation by through-going faults. The CRBG homocline forming the northwest margin of the Northern Willamette Basin is breached at Newberg, where

the GCF is inferred to cross the basin (Fig. 3 and Blakely et al., 2000). From Newberg to Canby, the southern margin of the CRBG shows three right-lateral separations of several km, one at the GCF, another at an unnamed fault west of Interstate 5, and one at the Canby fault (Fig. 4A).

The apparent offset of Columbia River Basalt Group (CRBG) homocline between Parrett Mountain and the Red Hills of Dundee at Newberg can provide an average post mid-Miocene slip rate (Figs. 4A and 4B). At Newberg, the southern margin of the CRBG is separated by 9.4–11.1 km in a right-lateral sense, depending on how much of the dextral bend in the contact is assumed to be related to fault offset. The Dundee Hills crest is also shifted ~6 km northwest of the trend of the Parrett Mountain crest, consistent with right-lateral offset of the CRBG. Using the age of the basalt (16 Ma) as the maximum time of tilting and an average apparent offset of 8.8 ± 2.5 km, the average, post-CRBG minimum dextral slip rate is ~0.55 ± 0.16 km/m.y. In the Washington Coast Range, the timing of major deformation of the CRBG postdates the 11–12 Ma Pomona flow of the Saddle Mountains Member of the CRBG (Magill et al., 1982; Wells et al., 2009). If tilting was post–11 Ma, the minimum average dextral slip rate would be at least 0.80 km/m.y. If all of the estimates are given equal weight, the average long-term geologic slip rate is 0.62 km/Ma, or 0.62 ± 0.12 mm/yr.

QUATERNARY ACTIVITY OF THE GALES CREEK FAULT

The geologic and geophysical evidence shows the GCF is a large fault with kilometers of dextral offset that could be accommodating some of the present northward displacement of the Coast Range indicated by GPS (McCaffrey et al., 2007, 2013). Bare-earth, high-resolution LiDAR topography acquired in 2009 by the Oregon Lidar Consortium reveals that nearly every stream crossing the fault is offset in a dextral sense, some nearly 2 km (Fig. 8A), and that the stream offsets coincide with the GCF strand showing bedrock offset of 12 km (Fig. 8B). The Willamette River at Newberg is also offset in a right-lateral sense where it crosses the fault zone. The smaller streams presumably date to the time of the uplift of the Coast Range. Estimates of uplift from stream incision (Personius, 1995) suggest the present Coast Range uplift may be as young as 2–3 m.y. If so, the dextral slip rate since 2–3 Ma could be as high as 0.6–1 mm/yr. On a smaller scale, first-order streams crossing the fault typically show tens of meters of dextral offset with small shutter ridges deflecting the stream (Fig. 8C). Although the geomorphology indicates youthful dextral slip, there are no dated Quaternary piercing points to determine a Quaternary slip rate.

Paleoseismic Investigations

The bare-earth airborne LiDAR data reveal discontinuous geomorphic scarps, breaks-in-slope, linear channels and valleys, and aligned apparent offset landforms along most of the GCF (Fig. 8). From these features, we identified three accessible scarp and lineament locations along the GCF to test for direct evidence of late Quaternary displacements along this fault zone. The first site, within Pacific University's Blodgett Arboretum (*BA* on Figs. 4A and 4B), is an apparent scarp aligned with the well-constrained bedrock trace of the GCF. Our second target, along the Parsons Creek strand of the GCF (*PC* on Fig. 4), appears as a lineament across gentle slopes and a slope break in steeper terrain. The third and ultimately most productive target was a ~6-km-long, mostly continuous lineament defined by scarps, drainage offsets, and aligned springs south of Cove Orchard (*CO* on Fig. 4). This fault appears to be a splay fault, possibly a reverse or thrust fault ~3 km southwest of the Chehalem Valley strand of the GCF.

Blodgett Arboretum

The Blodgett Arboretum site is situated in a small tract of Holocene fluvial terraces along Gales Creek in the foothills of the Coast Range (Fig. 4). These terraces occur where the GCF crosses its namesake stream (Fig. 9). The trace of the GCF is well constrained in the nearby bedrock on either side of Gales Creek and corresponds with an apparent 550 m right-lateral offset of the south wall of the Gales Creek Valley (Fig. 9). There is a suspicious lineament consisting of a 1–2-m-tall southwest-side-down topographic step that is aligned with the projection of the GCF across the fluvial terraces (Fig. 9). However, the modern channel of Gales Creek is also nearly parallel with the suspicious scarp, suggesting a potentially non-tectonic origin for the scarp. To resolve the ambiguity between geomorphic and tectonic origins of the scarp, we excavated a single trench across the scarp to expose the surficial deposits and to test for evidence of recent fault displacement (Figs. 9 and 10).

With limited space between trees at the site, we excavated a shallow, 12-m-long trench across the scarp, exposing sequences of fine-grained sediments overlying cobble-dominated terrace gravels (Fig. 10). The basal unit exposed in the trench is a clast-supported cobble and pebble-dominated gravel unit, labeled here as unit "tg" and interpreted as fluvial terrace gravel deposits (Fig. 10). The uppermost 10–20 cm of the deposit contains abundant interstitial silt and clay, creating strong cohesion between clasts. The underlying gravels are cohesionless where the silt and clay matrix is absent. Deposits overlying the terrace gravels are predominantly silt and fine sand (sts units) with discontinuous horizons of pebbles (peb) and coarser sand intervals. Capping the entire trench is a poorly sorted silt, sand, and pebble deposit that thins and becomes finer grained to the southwest in the trench. While initially mapped as colluvium (col; Fig. 10), we believe that this deposit is fill and reworked material produced during a variety of historic timber-related operations occurring along Gales Creek. The basal contact for this deposit is very wavy in the northeast half of the trench, perhaps attributable to the origin for the deposit.

No obvious fault trace occurs within the trench stratigraphy (Fig. 10). The basal contact for unit "col" is sharp and continuous; therefore, any earthquake rupture would have occurred prior to the deposition of this unit. Although the gravelly nature of deposits at the mid-trench step in terrace gravels could

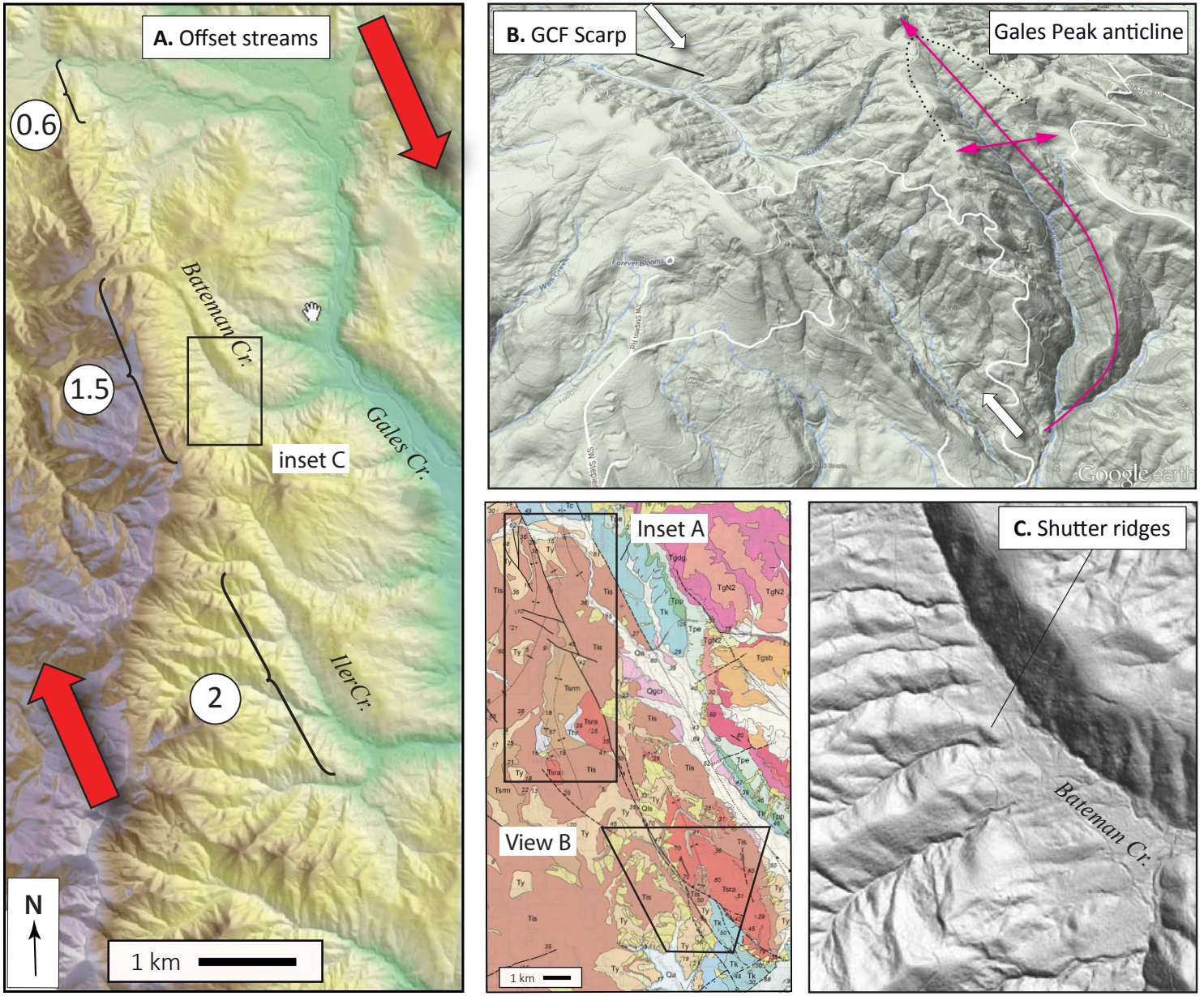

Figure 8. Evidence for Quaternary activity on the Gales Creek fault (GCF). (A) Light detection and ranging (LiDAR) topography reveals large right-lateral offset of streams crossing the GCF; offset in km, circled; (B) oblique Google Earth view of LiDAR topography showing linear GCF fault scarp between white arrows and axis of Gales Peak anticline; dotted line shows folded basalt flows; (C) shutter ridges. Geologic index map explanation as in Figure 4.

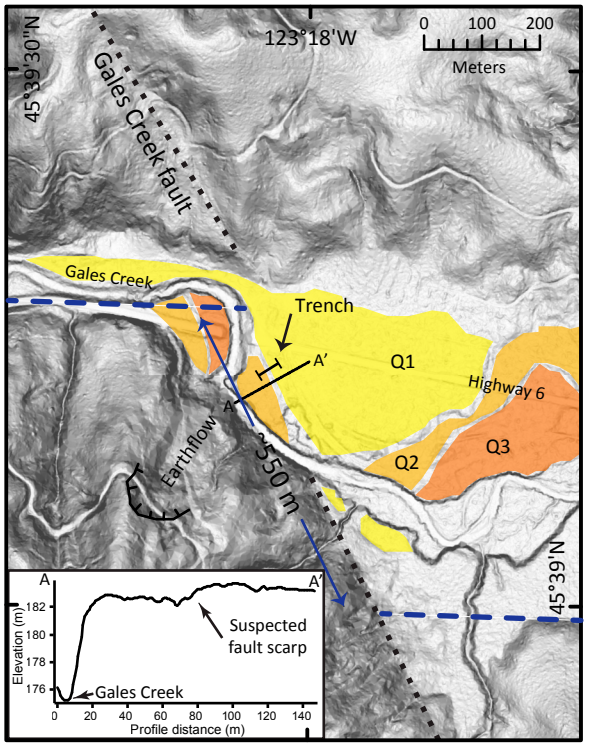

Figure 9. The Blodgett Arboretum trench site at the intersection of Gales Creek with the Gales Creek fault (GCF). A sequence of Holocene fluvial terraces occurs along Gales Creek, with Q1 representing the highest (oldest) fill surface, and Q2 and Q3 record subsequent incision and strath terrace formation. These fluvial deposits span the projection of the GCF with a topographic step between Q1 and Q2 (profile A–A′ on inset plot) aligned with the mapped trace of the fault. The south margin of the Gales Creek Valley displays an apparent ~550 m offset across the fault. Base image is a slope map derived from bare-earth airborne light detection and ranging (LiDAR) data from the Oregon Lidar Consortium.

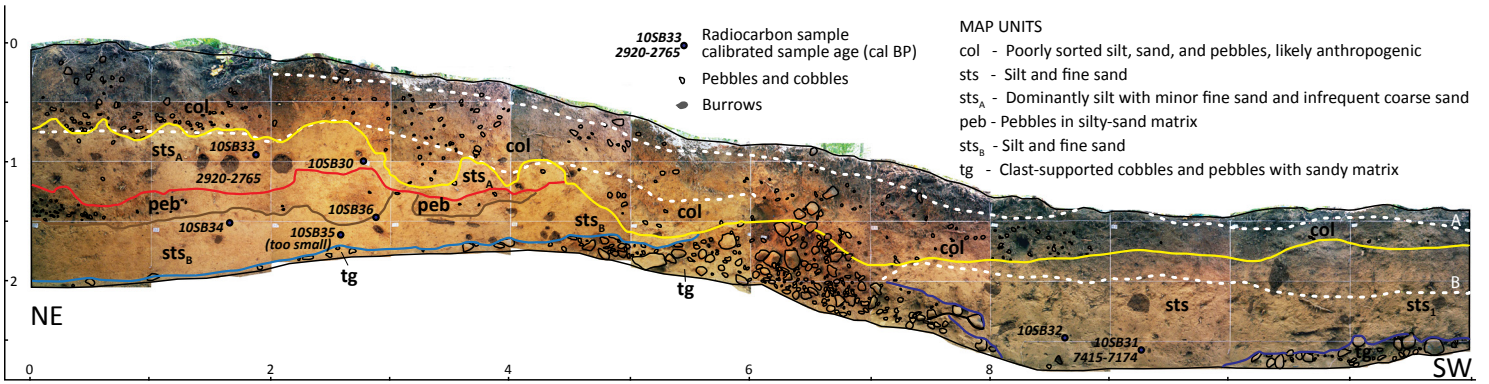

Figure 10. Southwest wall of the Blodgett Arboretum paleoseismic trench. Trench location shown on Figure 10. The stratigraphy consists of fluvial terrace gravels (tg) overlain by fluvial overbank deposits (sts units, peb); stratigraphy is in turn overlain by a deposit with a colluvial appearance (col) but likely includes anthropogenic fill and disturbed surficial deposits from timber and railroad operations during the late 1800s and early 1900s. Colored lines depict stratigraphic basal contacts; white dotted lines represent base of A and B soil horizons. To view a high-resolution image of the paleoseismic trench log in Figure 10, please visit https://doi.org/10.1130/GES02177.f10 or access the full-text article on www.gsapubs.org.

To view a high-resolution image of the paleoseismic trench log in Figure 10, please visit https://doi.org/10.1130/GES02177.f10 or access the full-text article on www.gsapubs.org.

TABLE 1. RADIOCARBON ANALYSES FROM THE GALES CREEK FAULT ZONE

Sample name*	Beta Analytic lab number	$\delta^{13}C$ (‰)	Fraction modern	$\delta^{14}C$	^{14}C age (yr B.P.)§	Calibrated age interval (yr B.P.)#	Sample material	Sampled unit
10SB33	292986	–25.3	0.7110 ± 0.0027	–289.0 ± 2.7	2740 ± 30	2920–2765	Charcoal	sts
10SB31B	292985	–24.3	0.4542 ± 0.0023	–545.8 ± 2.3	6350 ± 40	7415–7174	Charcoal	sts
SB10-25	292984	–25.6	0.8464 ± 0.0032	–153.6 ± 3.2	1340 ± 30	1306–1185	Charcoal	burrow
SB10-23	292983	–23.9	0.8602 ± 0.0032	–139.8 ± 3.2	1210 ± 30	1255–1059	Charcoal	burrow
SB10-20	292982	–24.5	0.8580 ± 0.0032	–142.0 ± 3.2	1230 ± 30	1262–1068	Charcoal	burrow

Note: Samples pretreated and analyzed by Beta Analytic, Inc.
*10SB33 and 10SB31B from Blodgett Arboretum site; SB10-25, -23, and -20 from Willakenzie Estate site.
§The quoted age is in radiocarbon years using the Libby half-life of 5568 years and following the conventions of Stuiver and Polach (1977). Sample preparation backgrounds have been subtracted, based on measurements of radiocarbon-dead standards pretreated in parallel with samples.
#Ages calibrated with Oxcal v. 4.2 (Bronk Ramsey, 2009) using the IntCal 13 calibration curve (Reimer et al., 2013), with ages quoted at 2σ errors.

obscure a fault trace, the sequences of fine-grained deposits do not represent offset equivalent units across the apparent scarp. We submitted three samples of detrital charcoal fragments for radiocarbon dating. One sample, 10SB35 (Fig. 10), was of insufficient size for analysis. The other two radiocarbon ages (Fig. 10 and Table 1) indicate that Gales Creek incised below the lower terrace gravels prior to 7415–7174 yr B.P. and that overbank deposition occurred across both surfaces through at least 2920–2765 yr B.P. Although potential ambiguity remains, we interpret this topographic scarp as a Holocene fluvial terrace riser because there is no clear evidence for a fault trace within the trench exposure, and a fault displacement is not required to create the observed stratigraphic relationships.

Parsons Creek

Parsons Creek is situated within the eastern foothills of the Coast Range and is a tributary of the Tualatin River (Fig. 4). The geomorphology of hillslopes in this region comprises three dominant forms: (1) landslide- and earthflow-dominated hillslopes, (2) steep, gullied hillslopes, and (3) smooth, convex ridge crests. For these hillslope forms, only the smooth convex slopes appear to have the potential of preserving prehistoric surface rupture traces. Two parallel topographic lineaments near Parsons Creek correspond with the previously mapped trace of the GCF, ~4.5 km north of Henry Hagg Lake (Fig. 4). These lineaments appear as small (submeter relief) scarps and aligned breaks-in-slope across relatively smooth hillslopes (Fig. 11). We examined these lineaments in the field for evidence of late Quaternary fault displacement. The northeastern scarp is positioned topographically higher and is characterized by a narrow, linear step across the hillslopes. The southwestern scarp appears predominantly as a break-in-slope, with the slope above being steeper than below (Fig. 11). We were unable to identify suitable markers for measuring displacement or determining the ages of offset landforms; however, a recent logging road cut across the southwestern scarp provided an exposure of the near-surface fault-related deformation (Figs. 12A and 12B). This exposure contains an abrupt fault contact between weathered mudstones of the Yamhill

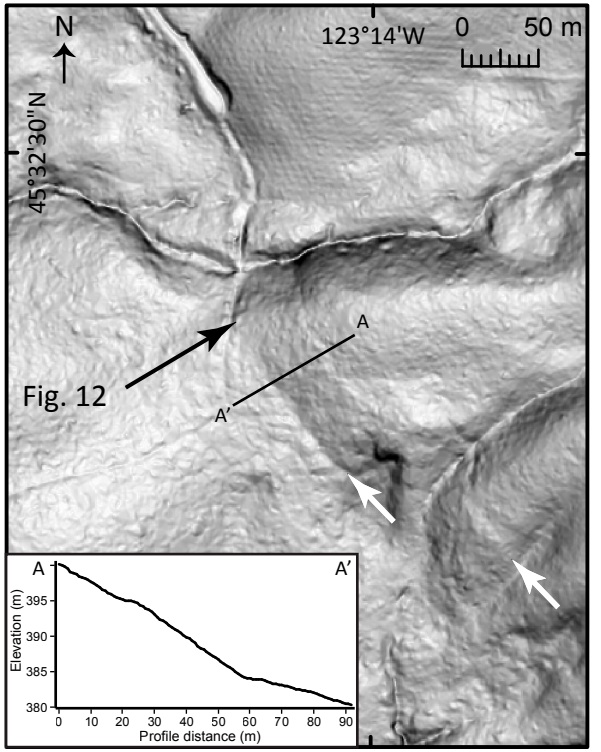

Figure 11. Gales Creek fault trace near Parsons Creek. Two NW-trending lineaments are apparent near the middle of the figure (white arrows), with the breaks-in-slope providing clear contrast on the grayscale slope map base derived from bare-earth light detection and ranging (LiDAR) digital elevation models. The small road cut shown by the black arrow crosses the lineament within a recently logged region, and the exposures found here are shown in Figure 13.

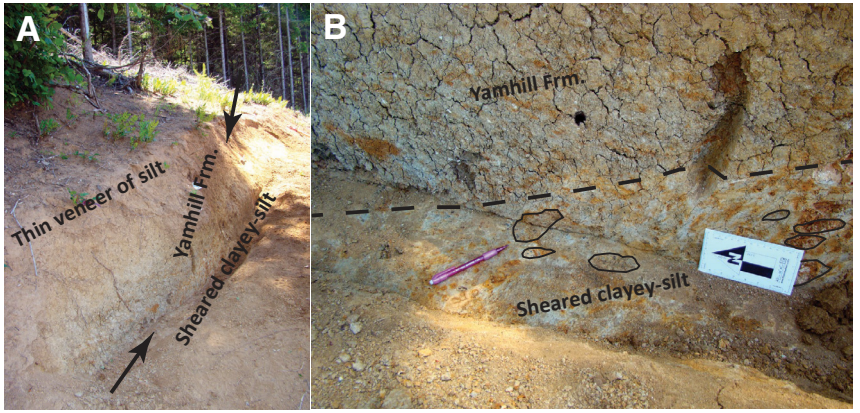

Figure 12. Road-cut exposure of the Gales Creek fault near Parsons Creek. (A) Shows fault in the cleaned surface of the road cut between the two black arrows. The surface of the site has been modified by logging and related activities, leaving no accessible surficial deposits intact across the fault trace. (B) Close-up of the fault, with a fault plane oriented 330°/30°NE juxtaposing deeply weathered Yamhill Formation mudstones over sheared clayey silt that contains small, lensoidal clasts of the Yamhill Formation (polygonal outlines show some of these clasts).

Formation and an unlithified clayey silt. The clayey silt is strongly sheared within the fault zone and contains lensoidal clasts of the Yamhill Formation (Fig. 12). The exposed fault is oriented 330°/30°NE, parallel to the scarp and the regional trace of the GCF.

The style of offset across the scarps and the geologic relationships exposed at Parsons Creek suggest a component of contraction across this portion of the GCF, bringing bedrock up in the hanging wall of what is a gently dipping fault near the surface. If the scarps preserve surface displacement rather than differential erosion along zones of weakness, then we suspect this fault has experienced a late Quaternary surface-rupturing earthquake.

Cove Orchard Faults

Subparallel to and 2–3 km southwest of the GCF zone is a distinct topographic lineament that is visible in bare-earth LiDAR topography for ~6 km. Numerous short ephemeral drainages cross the lineament, with several displaying apparent lateral offsets, but there is no systematic sense of offset from one drainage to the next (Fig. 12). This lineament did not correspond with any previously mapped faults (Wheeler et al., 2009) but is now interpreted to be a short splay of the GCF system (Figs. 4A and 4B). This lineament occurs on the northeast limb of a gently southeast-plunging anticline in tuffaceous mudstones of the Eocene Yamhill Formation, near the contact with the overlying Eocene micaceous sandstone of the Cowlitz Formation. Our paleoseismic investigations targeted a site near the southern end of the lineament due to the correspondence of a well-defined, discrete trace with easy site access. The lineament has two parallel traces ~400 m in length; we chose a gentle ridge crest with no indications of recent slope movement for our trench site.

Paleoseismic Trench Descriptions. Our initial trench crossed the southern lineament, which is defined here by an ~9° break-in-slope (Fig. 13). This 18-m-long trench was oriented at ~030°NE, near perpendicular to the lineament and excavated to ~1.5 m depth. We cleaned and prepared both trench walls for logging (Fig. 14A). Our second trench was excavated parallel to Trench 1 but offset 2 m to the northwest and extending an additional 6 m uphill across the northern lineament with 4 m of overlap with the northeast end of Trench 1 (Figs. 13 and 14B). This trench was 10 m long with a vertical wall up to 2.5 m tall and a benched opposite wall with only the vertical wall prepared for logging (Fig. 14B). With the close proximity and stratigraphic and structural overlap between the two trenches, we describe these trenches as a continuous exposure, defining the horizontal scale of Figures 14A and 14B from 0 m at the N end of Trench 2 to 24 m at the S end of Trench 1.

The units exposed in these trenches consist primarily of deeply weathered tuffaceous mudstones of the Eocene Yamhill Formation. Superimposed upon the bedrock are two well-defined soil horizons in the upper 40–80 cm, with the A horizon defined by the presence of fine-grained organic material, a lack of Yamhill Formation clasts, and blocky soil structure. The B horizon is distinguished by abundant, randomly oriented clasts of Yamhill Formation mudstone in a clayey-silt matrix with numerous filled burrows. The only other distinct stratigraphy in these trenches comprises two packages of clayey silt and a discrete zone of colluvial deposits. A near-horizontal, 40-cm-thick bed of clayey silt is preserved between meters 5–10 (clst1) and irregularly shaped blobs, lenses, and horizons of a similar clayey silt occurs in the southern end of Trench 1 from meter 16 to the end of Trench 1 (clst2; Fig. 14A). The colluvial deposits are generally composed of small Yamhill Formation fragments in a clayey-silt matrix and overlie unit clst1 in both trenches (Figs. 14A and 14B). A portion of these colluvial deposits, exposed between meters 5–7 in Trench 2 (Fig. 14B), preserves weak bedding defined by variations in clast sizes and the fraction of silt and/or clay. Across meter 7, the bedding ends and the colluvial deposits transition into an unsorted deposit of small Yamhill Formation clasts in a silt and/or clay matrix that is deposited directly on top of unit clst1

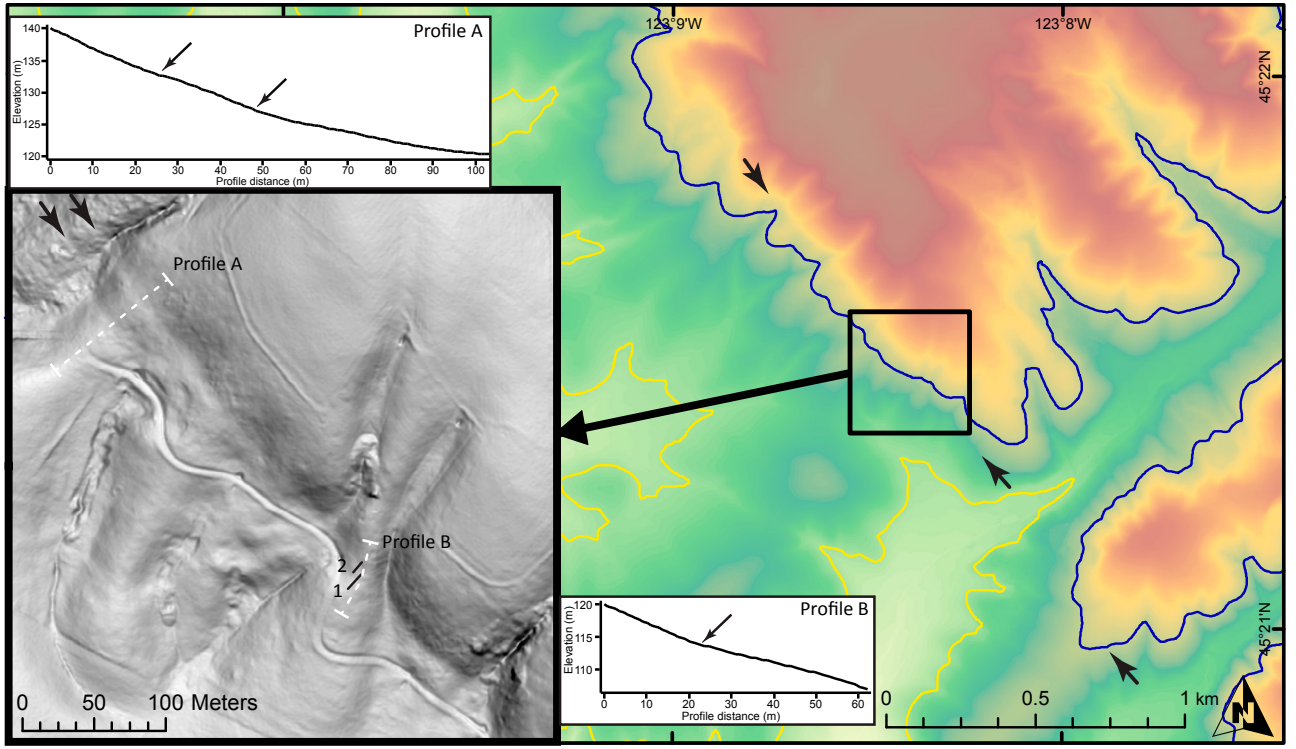

Figure 13. The Cove Orchard paleoseismic site on the Gales Creek fault (GCF) system (location CO on Fig. 4). A previously unrecognized northwest-trending lineament (illustrated with black arrows) corresponds with a northwest-trending topographic step subparallel to the main GCF. Blue and yellow contours define inundation levels from the late Pleistocene Missoula floods in the Willamette Valley, with the blue contour defining the highest inundation level (122 m) and yellow defining the elevation reached by ten or more separate floods (Minervini et al., 2003). Base imagery is a grayscale slope map with a color elevation overlay on the main figure.

(Fig. 14B). These appear to be two generations of colluvial deposits, as the bedded colluvial deposits are folded and in fault contact with unit clst1 below, whereas the unsorted colluvial deposits occur at and downslope from the fault tip, indicating these are the youngest, scarp-derived colluvial deposits.

The deformation style and orientations of structures vary along the length of the exposure. In the northeastern end of Trench 2, from meters 0–4, deformation appears as 5–10-cm-wide zones of crushed and rotated mudstone fragments. These zones dip gently to the northeast and southwest but are irregular and discontinuous. Between meters 3.5–7, there is a well-defined, northeast-dipping fault zone that places Yamhill Formation mudstone over unit clst1 (Fig. 14B). Two primary fault traces consist of 2–6-cm-thick, gray sheared clay bands that merge up-dip into a single fault plane. The fault becomes near horizontal at meter 6, and the shear fabric associated with this fault diminishes near meter 7, where it appears to transition into a depositional contact of colluvium on unit clst1. We measured slickenline orientations of 036°/20°NE on slip planes within a fault plane oriented 309°/21°NE, indicating primarily reverse displacement. Between meters 9–16 (Fig. 14A), the relatively homogeneous disaggregated mudstone contains numerous, narrow (<5 cm), moderately northeast-dipping shear zones where the mudstone fragments are crushed and rotated. These shear zones end abruptly at a subvertical fault zone near meter 16. Consisting of several anastomosing 1–3-cm-wide clayey shear zones, this fault is parallel to the fault near meter 5, but we were unable to identify kinematic indications of slip orientation from the shear zones. From meter 16 to the southwest end of Trench 1, the structure is complex with blocks and bodies of disaggregated mudstone separated by clay-rich horizons and irregularly shaped blobs of silty clay. The blocks of mudstone all occur above an undulating but overall subhorizontal clay-rich horizon. Below this horizon is relatively intact Yamhill Formation mudstone with weak bedding oriented

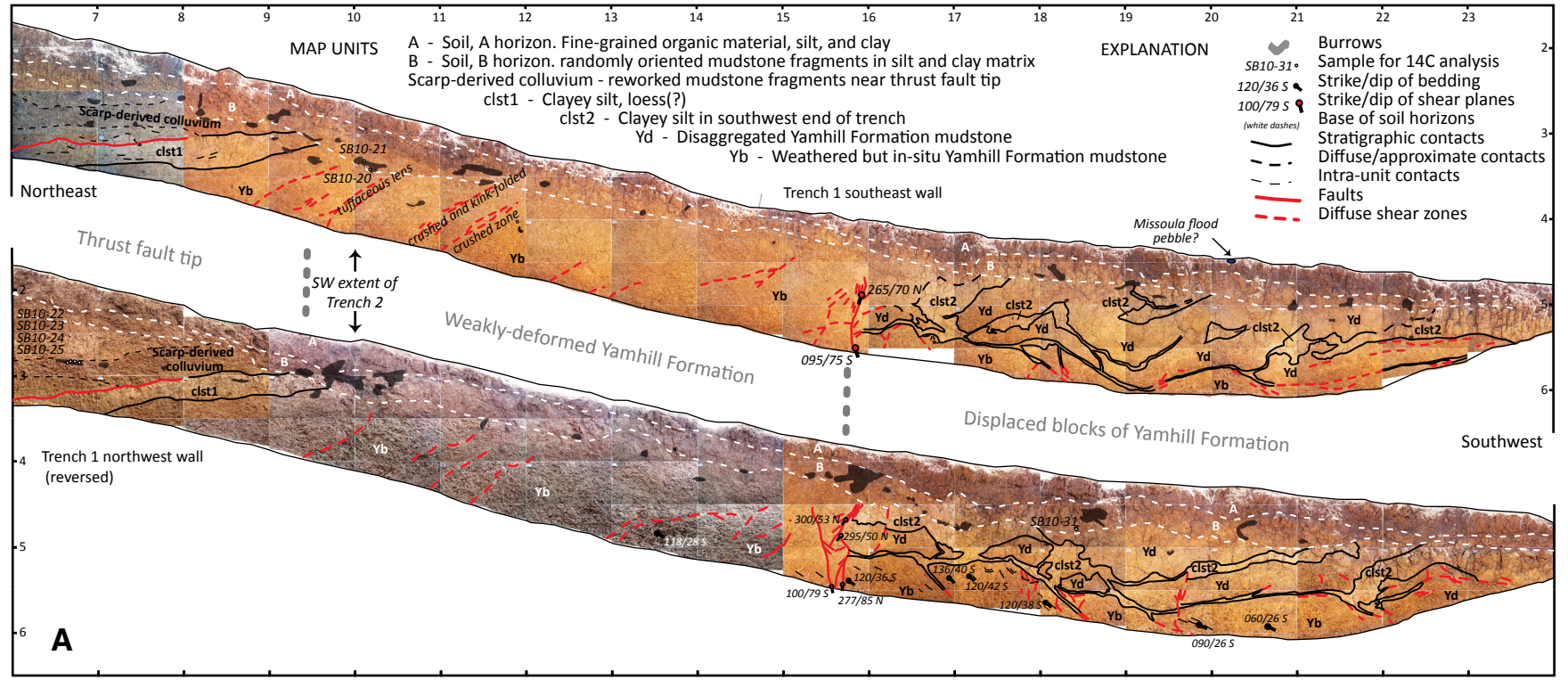

Figure 14. (A) Photomosaics and logs of Trench 1 at the Cove Orchard site. Both walls of the trench are shown, with the northwest wall flipped so they are displayed in the same orientation. This trench displays three structural and stratigraphic zones, with the northeast end capturing a portion of the fault surface that places bedrock and colluvium over the former ground surface, the middle of the trench composed of weakly deformed Eocene Yamhill Formation mudstone, and the southwest end exhibiting a shallow slip surface that translates blocks of mudstone downslope. The soil horizons are undeformed and overprint the preexisting stratigraphic relations. To view high-resolution images of paleoseismic trench logs in Figure 14A, please visit https://doi.org/10.1130/GES02177.f14a or access the full-text article on www.gsapubs.org. (*Continued on following page.*)

To view high-resolution images of paleoseismic trench logs in Figure 14A, please visit https://doi.org/10.1130/GES02177.f14a or access the full-text article on www.gsapubs.org.

~120°/40°S. Several shear zones penetrate below the subhorizontal clay-rich horizon and are mostly parallel to local bedding (Fig. 14A).

Structural Interpretation. The fault zones at meters 5 (Fig. 14B) and 16 (Fig. 14A) in these trenches appear to be the only faults that are both deep rooted and exhibit appreciable displacement. In particular, the thrust fault at meter 5 records evidence of at least one prehistoric surface-rupturing earthquake, where it places Yamhill Formation mudstone and older colluvium over unit clst1. We interpret clst1 to represent the ground surface at the time of the earthquake, because it is a well-sorted clayey silt that unconformably overlies the Eocene Yamhill Formation and because the shear plane of the fault becomes bedding parallel at the top of the unit and transitions into a depositional contact. Although weathering and minor shearing obscure the depositional character of clst1, we interpret it as a loess. The colluvial unit between meters 6.5–10 represents a post-earthquake, scarp-derived colluvial deposit that buried the ground surface beyond the fault tip at the time of or soon after the earthquake. Displacement on the subvertical fault at meter 16 likely produced the complex structures between the fault and the southwest end of Trench 1. Most of the deformation in this zone occurs above the undulating subhorizontal clay-rich horizon, which appears to have acted as a detachment in accommodating a small amount of downslope (southwest) movement of the hanging wall. The shapes of the mudstone blocks overlying this detachment can be matched puzzle-like by back-slipping each block upslope on the order of 5–30 cm.

Age Control. With most of the stratigraphy composed of Eocene Yamhill Formation, targets for direct Quaternary age control consisted of organic materials in the upper ~0.5 m of the section (within the soil horizons) and from the unit clst1. Numerous burrows penetrate below the A horizon and contain charcoal fragments. Several burrows along the A/B horizon boundary provide

To view high-resolution images of paleoseismic trench logs in Figure 14B, please visit https://doi.org/10.1130/GES02177.f14b or access the full-text article on www.gsapubs.org.

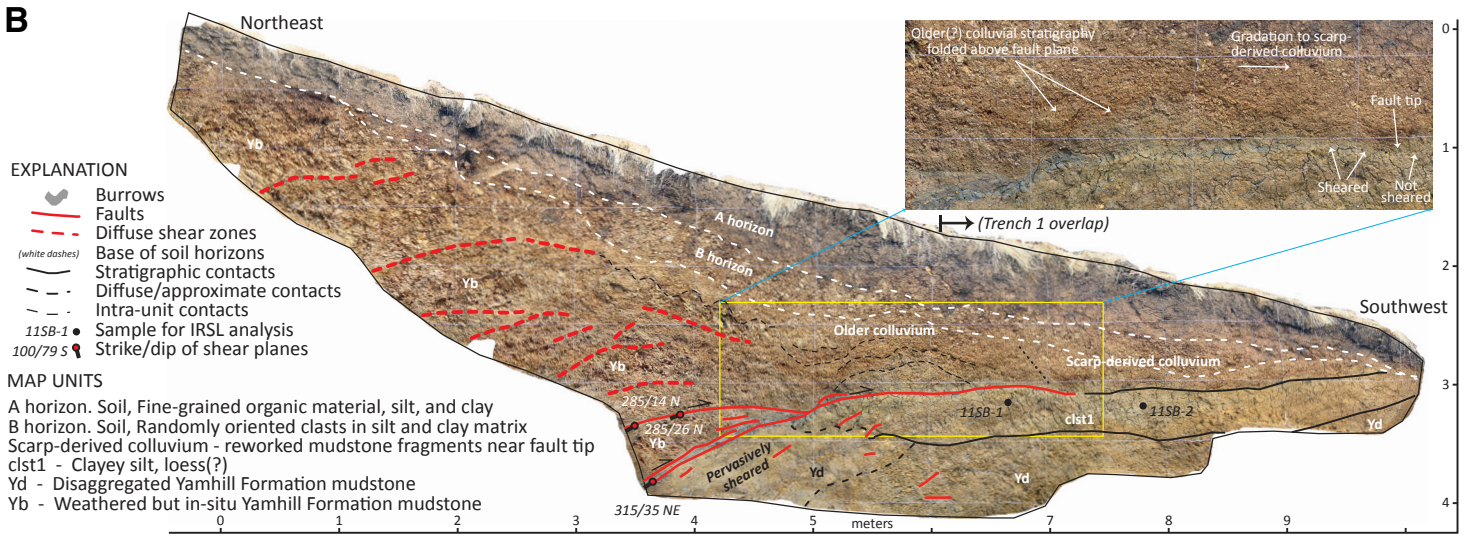

Figure 14 (*continued*). (B) Southeast wall of the second paleoseismic trench at the Cove Orchard site. The southwestern 4 m of this trench overlap with the northeastern end of Trench 1 (Fig. 6A), which was parallel to this trench and offset 2 m to the southeast (behind this exposure). The exposed stratigraphy consists primarily of deeply weathered and reworked and/or deformed Yamhill Formation, except for where a north-dipping thrust fault places Yamhill Formation over an ~40-cm-thick package of clayey silt (clst1) dated at ~250,000 yr B.P. (Table 2). This clayey silt is interpreted to be the preserved ground surface from the time of a surface-rupturing earthquake. IRSL—infrared stimulated luminescence. To view high-resolution images of paleoseismic trench logs in Figure 14B, please visit https://doi.org/10.1130/GES02177.f14b or access the full-text article on www.gsapubs.org.

consistent radiocarbon ages of ca. 1200 yr B.P. (Table 1). There is no evidence of offset or deformation of the soil horizons containing these burrows, thus providing a minimum age for the most recent surface-rupturing earthquake on this fault. An additional, albeit indirect, control on the minimum age of the most recent earthquake is the occurrence of hard, rounded, subcentimeter-sized exotic clasts that occur in the uppermost 5 cm of the A horizon. These clasts are inferred to be dropstones from the highest of the late Pleistocene Missoula floods that inundated the Willamette Valley as recently as ca. 16 ka (Fig. 13; Minervini et al., 2003).

To establish age control for the ground surface prior to the earthquake, we collected two samples from unit clst1 (Fig. 14B) for infrared stimulated luminescence (IRSL) dating (Table 2). We interpreted unit clst1 to be a loess deposit. It is composed of massive, structureless, well-sorted silt (with secondary clay formation), and we sampled the silt fraction for luminescence dating. Both samples were repeatedly centrifuged to separate the clay and silt fractions, with everything <10 microns in size discarded and analyses conducted on the 10–15-micron-size fraction (no larger grains were present). Samples 11SPB-1 and 11SPB-2 were collected from approximately the same stratigraphic level within unit clst1 (Fig. 14B), and these samples produced ages of 280,000 ± 27,000 yr B.P. and 250,000 ± 23,000 yr B.P., respectively (Table 2). These samples provide consistent estimates of the age of the unit and suggest that this deposit formed during Marine Isotope Stage 8. These luminescence ages for unit clst1 indicate that the most recent earthquake on this splay fault occurred <~250 k.y. ago.

DISCUSSION

The GCF, with ~12 km of right-lateral offset since 35 Ma, is the largest strike-slip fault yet recognized in the Cascadia forearc of Oregon and Washington. The fault has a long history extending back to the Eocene, given that the fault bounds an apparent Tualatin pull-apart basin, filled in part with Paleogene sedimentary rocks. Locally, along the Gales Creek strand, the late Eocene shallow marine arkose of the Cowlitz Formation is missing on the Gales Peak anticline, with the basal late Eocene shelf sandstone of the Keasey Formation overlying slope mudstone of the Yamhill Formation on a regional unconformity (Fig. 4B). Some of the 12 km offset of the Gales Peak anticline may be Paleogene, as the average right-lateral separation of the 16 Ma CRBG is less, ~8.8 km at Newberg.

Relation to Other Forearc Faults

The large right-lateral offset indicates the GCF is part of a major fault system that likely extends beyond the 60 km mapped length in this report. The

TABLE 2. INFRARED STIMULATED LUMINESCENCE POLYMINERAL DATA AND AGES FROM COVE ORCHARD PALEOSEISMIC TRENCH

Sample name	% water content[a]	K (%)[b]	U (ppm)[b]	Th (ppm)[b]	Cosmic dose additions (Gy/ka)[c]	Total dose rate (Gy/ka)	Equivalent dose (Gy)	Age (yr)[d]
11SPB-1	28 (93)	0.85 ± 0.04	1.42 ± 0.12	4.88 ± 0.32	0.19 ± 01	1.61 ± 0.08	448 ± 4.48	280,000 ± 27,480
11SPB-2	32 (83)	0.82 ± 0.04	1.38 ± 0.10	5.00 ± 0.29	0.18 ± 0.01	1.65 ± 0.07	413 ± 4.13	250,000 ± 22,970

Note: Sample preparation and analyses conducted at the U.S. Geological Survey Luminescence Dating Laboratory.
[a]Field moisture values with figures in parentheses indicate the complete sample saturation % (very expansive clays). Ages calculated using 60% of full saturation value.
[b]Analyses obtained using gamma spectrometry (Ge detector).
[c]Cosmic doses and attenuation with depth were calculated using the methods of Prescott and Hutton (1994).
[d]Dose rate and age for fine-grained 10–15 microns polymineral silt (infrared stimulation on K-feldspars). Exponential fit used on equivalent dose, errors to one sigma.

geomorphic and paleoseismic evidence for Quaternary activity on the western strands of the GCF defines a complex, multi-strand system characterized by restraining bend geometry that projects southward into the Northern Willamette Basin at Newberg. The structures at Newberg align with aeromagnetic anomalies along the Mount Angel fault (MAF, Fig. 3) and related structures in the subsurface. These subsurface structures extend southward across the valley and show similar restraining bends in the source area of the 1993 M 5.7 Scotts Mills earthquake (Blakely et al., 2000). Our observations of GCF geometry and potential activity provide a surface analog directly along strike with the subsurface geometry proposed for the MAF and are consistent with GCF-MAF links proposed by Beeson et al. (1989a) and Blakely et al. (2000). Although no surface trace of the MAF is known, the Scotts Mills earthquake and prolonged background seismicity along the fault and related structures indicate the MAF is seismically active.

The eastern strand of the GCF along Gales Creek, in contrast, appears to connect to faults in the Tualatin Basin (Fig. 15). Wells et al. (2019) used water well log databases of Madin (1990), Gannett and Caldwell (1998), and Wilson (1997, 1998), supplemented by additional logs from the Oregon Water Resources Department (2017) to locate the top of the Miocene Columbia River Basalt Group (CRBG) beneath the Tualatin Basin (data in Wells et al., 2019 geodatabase). There is an apparent offset in the CRBG of ~150 m, north side down, which extends westward from Beaverton to the GCF, ~25 km (Wells et al., 2019). We interpret this step to be the Beaverton fault as described by Madin (1990), and we suggest the Beaverton fault links the GCF to the Canby fault to the southeast (Fig. 15). The Beaverton fault is interpreted as a thrust or reverse fault separating the east-striking Cooper Mountain anticline in the hanging wall from the synclinal basin axis in the footwall (Madin, 1990; Yeats et al., 1996). The top of CRBG in the basin center is ~1200 ft (370 m) below sea level (Yeats et al., 1996; Wilson, 1997), much less than the 5 km basin depth from the gravity inversion. Seismic data (Oregon Department of Geology and Mineral Industries, 2012) show the Beaverton fault accommodates some of the large vertical offset of Siletz basement into the basin at its western end and indicates a probable link to GCF at Forest Grove.

Our geologic mapping and interpretation of the depth to the top of the CRBG (Fig. 15) reveal the Cooper Mountain anticline to be one of a series of east-west ridges and adjacent subsurface troughs beneath the southern basin. Wilson (1997) interpreted these structures as horsts and grabens, but we interpret them as anticlines and synclines in the hanging wall of the Beaverton fault, consistent with the fold structure of Cooper Mountain and the current N-S maximum horizontal compressive stress field from seismicity and well-bore breakouts (Werner et al., 1991; Fig. 15). The water well data suggest that the folds and the Beaverton fault are offset by a series of northwest-trending dextral faults subparallel to the GCF. The inferred dextral faults and their offsets coincide with right-lateral bends in the Tualatin River and with truncations of fold axes in CRBG mapped at the surface. Under Fanno Creek (south of Beaverton, Fig. 4A), similar truncations (Fig. 4B) are interpreted to mark a dextral fault that connects with the Canby fault, making it 40 km long. In this interpretation, the Beaverton fault and the subparallel folds are a 30-km-wide compressive step-over between the Canby fault and CGF-MAF fault systems. These folds and faults are geometrically similar to the Yakima folds in central Washington, with long backlimbs, tight or missing forelimbs, and locally offset by transverse right-lateral faults (cf. Tolan and Reidel, 1989). The Beaverton fault lacks clear geomorphic evidence for recent surface rupture. However, the Tualatin River, in its meandering path through the basin, cuts straight through the Beaverton fault and its related folds (Fig. 4A), suggesting possible tectonic control of river incision by uplift on the fault.

A precise GPS estimate of the slip rate on the GCF cannot be determined at this time, given the probable low slip rate, less than optimum station spacing, and the overwhelming signal from locking on the Cascadia megathrust (R. McCaffrey, 2019, personal commun.). If we assume the long-term slip rate is valid, the broader northwest-trending GCF-MAF-PHF fault system could accommodate northward motion of the Cascadia forearc at a long-term (post–15 Ma) geologic rate of ~0.9 mm/yr, if we add an estimated post–1 Ma dextral component on the NW-striking Sylvan-Oatfield fault exposed in the light rail tunnel through the Portland Hills (Walsh et al., 2011). This geologic rate is consistent with regional GPS results that indicate ~1.5 mm/yr north-directed dextral shear across western Oregon (McCaffrey et al., 2007) and fits models of distributed lithospheric shear based on the increase in clockwise paleomagnetic rotation toward the coast (England and Wells, 1991).

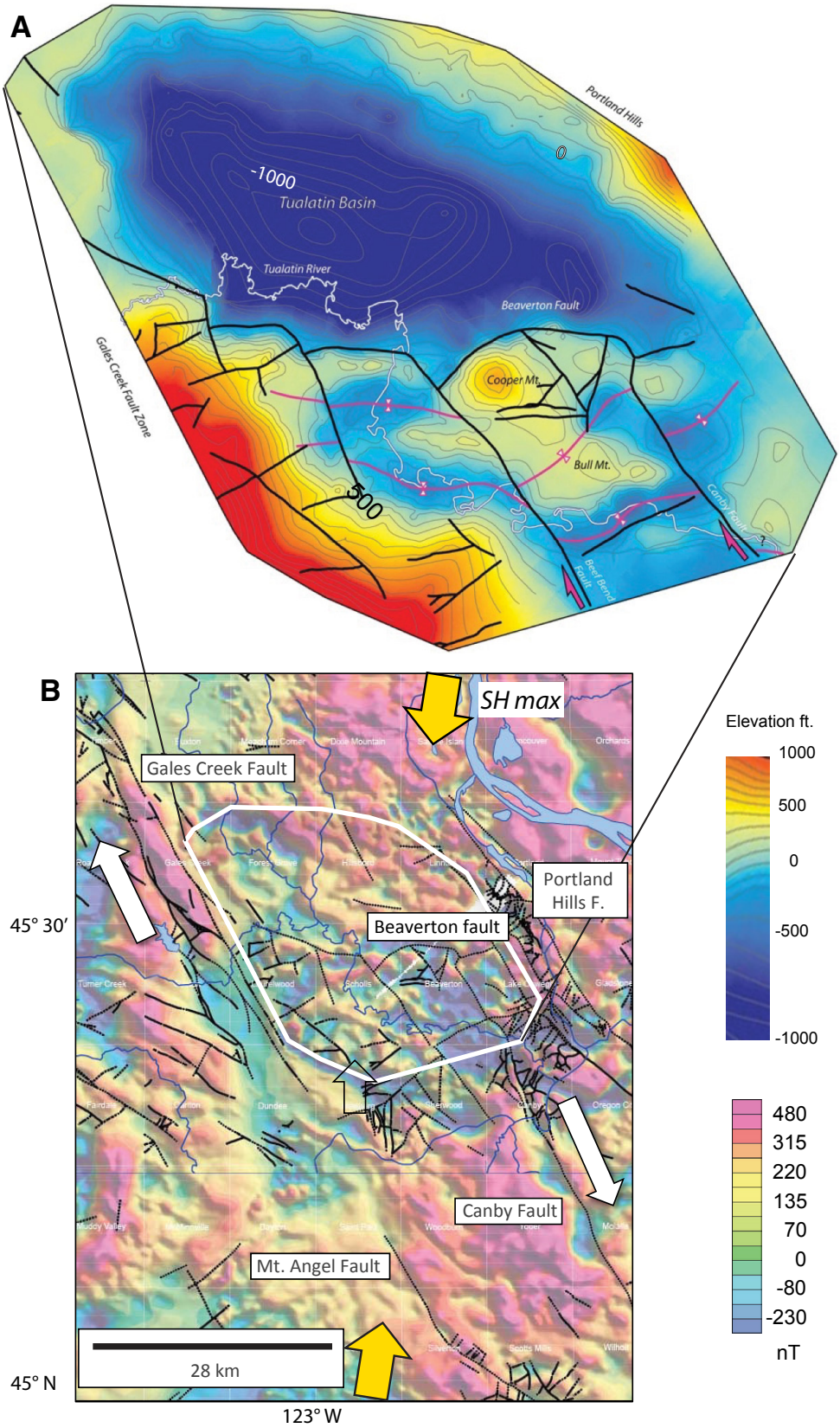

Figure 15. (A) Elevation of the top of Columbia River Basalt Group (CRBG) in Tualatin Basin, in feet above mean sea level. CRBG is more than 1200 ft (366 m) below sea level in the center of the basin. Beaverton fault bounds Yakima-style fold belt across southern basin. (B) Location of Tualatin Basin on aeromagnetic anomaly map with crustal faults. Compressive step-over links right-lateral Gales Creek fault to Portland Hills–Canby fault system (white arrows) through Beaverton reverse fault and CRBG fold belt in its hanging wall. Maximum horizontal stress direction (SH max) from Werner et al. (1991) shown by yellow arrows.

Relation to Forearc Rotation

In northwest Oregon and southwest Washington, the westward increase in rotation is accommodated by a distinctive pattern of rotating, N60°–70°W sinistral, R′ faults that form domino-style domains bounded by larger NNW dextral faults (Fig. 16; Wells and Coe, 1985; Wells et al., 1995; see Freund, 1974 for an analysis of domino, or bookshelf style faulting). This pattern of faulting extends offshore to the deformation front (Goldfinger et al., 1997). In northwest Oregon, the GCF forms the eastern boundary of a similar Coast Range domain of sinistral faults, some with kilometers of offset, that extend westward to the coast (Wells et al., 1995). This fault pattern may accommodate up to half of the observed rotation. Using the spacing and apparent offset of the largest sinistral faults (e.g., Tillamook Bay) with 20 km left separation and the Nehalem River fault system 40 km to the north, the fault geometry could accommodate 47% of the 46° clockwise rotation of the Tillamook Volcanics (Fig. 16). The left-stepping restraining bend geometry of the GCF-MAF-PHF fault system is similar to the Willapa Hills fault system in southwest Washington (Wells and Coe, 1985; Wells and Sawlan, 2014; Blakely et al., 2016), and it accommodates clockwise rotation and N-S shortening as the forearc moves northward relative to North America (Fig. 16).

Relation to Seismicity and Magmatism

Our interpretation of the Tualatin Basin as an Eocene pull-apart basin undergoing structural inversion to N-S shortening (Fig. 8) in post-CRBG time (since 15 Ma) is consistent with a pattern of left-stepping restraining bends in the GCF described here, and in the Willapa Hills of southwest Washington (Wells and Coe, 1985). North-northwest alignments of seismicity in the forearc and arc (e.g., Mount St. Helens seismic zone and similar features; Brocher et al., 2017) are also consistent with northward motion of the Coast Range, but in contrast to the geology, epicenter lineaments step right (Fig. 16, e.g., GCF, PHF, SHSZ, and W. Rainier seismic zones), forming releasing bends along the weaker crust of the arc.

Another apparent paradox is the relation of the dextral GCF-MAF-PHF fault system to the basaltic lavas of the Boring Volcanic Field in the Portland and Tualatin Basins (Evarts et al., 2009). Beeson et al. (1989a, 1989b) proposed that the basins were extensional pull-apart basins that provided a path to the surface for the mafic magma. Fleck et al. (2014) showed that Boring vents migrate northwest at ~9 mm/yr, and their alignment rotates clockwise over time. They suggested that the vents were tracking the northward motion of the Oregon Coast Range block. The apparent paradox could be explained if crustal seismicity is time dependent and is affected by the megathrust seismic cycle, and is therefore not completely capturing long-term fault motion (Stein, 1999; Sevilgen et al., 2012).

We can consider dextral shear of the forearc as an overprint of Pacific–North America shear on the structure and processes of subduction. The GCF system

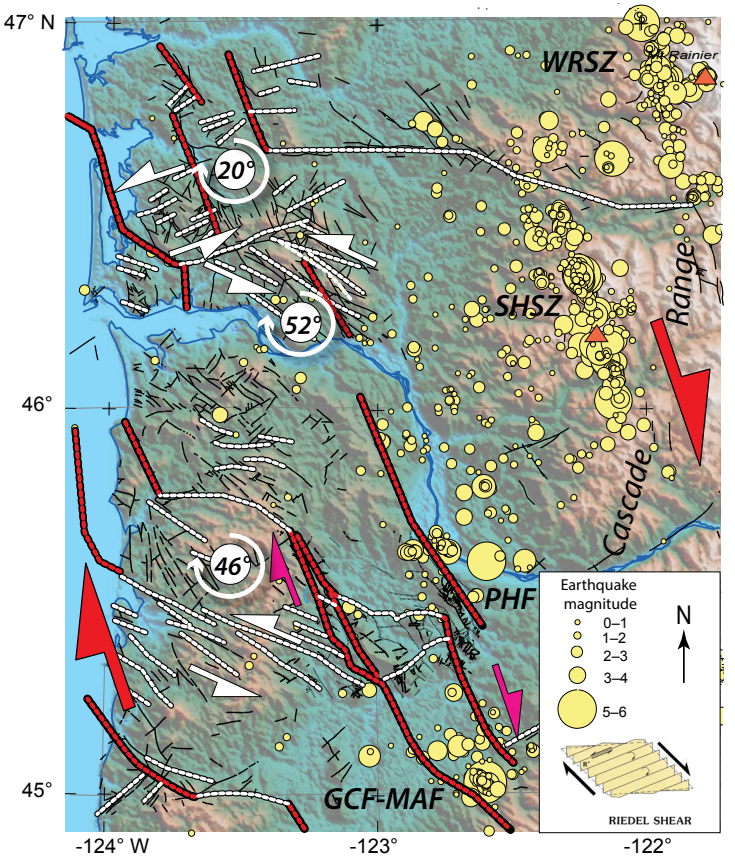

Figure 16. Crustal seismicity and faults in the NW Oregon and SW Washington forearc, modified from the state geologic maps of Washington (Schuster, 2005), Oregon (Walker et al., 2003), and Wells et al. (2019). Forearc faults form left-stepping arrays of right-lateral faults (red lines) bounding domains of WNW- and ENE-striking left-lateral faults (white dotted lines) that accommodate up to half of the 46° clockwise rotation of the Coast Range (Magill et al., 1981; see also Wells and Coe, 1985 for SW Washington). In contrast, seismicity from the Pacific Northwest Seismic Network steps right, following the volcanic arc, and suggesting releasing bend geometry. Inset shows idealized model of brittle shear rotation by R′ faults (Freund, 1974) and earthquake magnitude scale; see text for additional discussion.

is one of several dozen large faults that bound rotating blocks and accommodate northward motion of the forearc. Forearc faults such as the GCF partition the margin-parallel component of subduction into permanent deformation of the upper plate. Work in progress by Redwine et al. (2017, 2019) and Horst et al. (2018, 2019) has documented multiple Holocene earthquakes on the Scoggins and Chehalem Valley strands below Scoggins Dam and on the Parsons Creek strand north of Hagg Lake. The main, 60-km-long Gales Creek segment is

capable of a Mw 7.3 earthquake if the entire segment were to rupture at once (Stirling et al., 2013). Given geophysical links to the MAF and the PHF, it could potentially generate a larger, complex, multi-segment earthquake.

CONCLUSIONS

The GCF is a northwest-trending dextral fault system (west of Portland, Oregon) that accommodates northward motion and uplift of the Coast Range. Geologic offset of Siletzia basement and its aeromagnetic anomalies are at least 10–12 km in a right-lateral sense since 35 Ma, and offset of Columbia River Basalt Group flows at Newberg is ~8.8 km since 16 Ma (~0.4–0.6 mm/yr). Geologic mapping shows Eocene Siletz basement exposed in the Coast Range west of the fault is buried beneath 5 km of sediment in the Tualatin Basin to the east, consistent with gravity models. The 60-km-long main segment of the GCF is linked to the Mount Angel and Portland Hills–Canby right-lateral fault systems through a set of compressive step-overs, including the Beaverton fault, that accommodate north-south shortening of the forearc.

Progressive, clockwise rotation of the forearc is accommodated by subordinate sinistral faults that rotate domino-style between the right-lateral faults. The long-term geologic slip rate is about one-third of the 1.5 mm/yr dextral shear in western Oregon previously inferred from GPS data. LiDAR data reveal offset streams, shutter ridges, scarps, and other youthful geomorphic features for 40 km along the geophysical and geologic trace of the fault. Two of three paleoseismic trenches described here indicate late Quaternary activity on the GCF. A reverse splay of the fault east of Yamhill reveals Eocene bedrock thrust over a surficial silt deposit with an optically stimulated luminescence date of ~250,000 years, indicating an earthquake in late Quaternary time.

ACKNOWLEDGMENTS

We thank Lydia Staisch, Andrew Meigs, and two anonymous reviewers for very helpful comments on an earlier version of this manuscript.

REFERENCES CITED

Barnett, E.A., Haugerud, R.A., Sherrod, B.L., Weaver, C.S., Pratt, T.L., and Blakely, R.J., compilers, 2010, Preliminary atlas of active shallow tectonic deformation in the Puget Lowland, Washington: U.S. Geological Survey Open-File Report 2010-1149, 32 p., 14 maps.

Beck, M.E., Jr., 1976, Discordant paleomagnetic pole positions as evidence for regional shear in the western Cordillera of North America: American Journal of Science, v. 276, p. 694–712, https://doi.org/10.2475/ajs.276.6.694.

Beck, M.E., Jr., 1980, Paleomagnetic record of plate-margin tectonic processes along the western edge of North America: Journal of Geophysical Research, v. 85, p. 7115–7131, https://doi.org/10.1029/JB085iB12p07115.

Beeson, M.H., Tolan, T.L., and Anderson, J.L., 1989a, The Columbia River Basalt Group in western Oregon—Geologic structures and other factors that controlled flow emplacement tectonism in the Columbia River flood-basalt province, *in* Reidel, S.P., and Hooper, P.R., eds., Volcanism and Tectonism in the Columbia River Flood-Basalt Province: Geological Society of America Special Paper 239, p. 223–246, https://doi.org/10.1130/SPE239-p223.

Beeson, M.H., Tolan, T.L., and Madin, I.P., 1989b, Geologic map of the Lake Oswego quadrangle, Clackamas, Multnomah and Washington Counties, Oregon: Oregon Department of Geologic and Mineral Industries Geological Map Series BMS-59, 1:24,000.

Blakely, R.J., 1995, Potential Theory in Gravity and Magnetic Applications: Cambridge, UK, Cambridge University Press, 441 p.

Blakely, R.J., Wells, R.E., Yelin, T.S., Madin, I.P., and Beeson, M.H., 1995, Tectonic setting of the Portland-Vancouver area, Oregon and Washington: Constraints from low-altitude aeromagnetic data: Geological Society of America Bulletin, v. 107, no. 9, p. 1051–1062, https://doi.org/10.1130/0016-7606(1995)107<1051:TSOTPV>2.3.CO;2.

Blakely, R.J., Wells, R.E., Tolan, T.L., Beeson, M.H., Tréhu, A.M., and Liberty, L.M., 2000, New aeromagnetic data reveal large strike-slip (?) faults in the northern Willamette Valley, Oregon: Geological Society of America Bulletin, v. 112, p. 1225–1233, https://doi.org/10.1130/0016-7606(2000)112<1225:NADRLS>2.0.CO;2.

Blakely, R.J., Wells, R.E., Sherrod, B.L., and Brocher, T.M., 2016, Segmentation of the Cascadia forearc in southwestern Washington—Evidence from new potential-field data: American Geophysical Union, Abstract GP34A-04.

Brocher, T.M., Wells, R.E., Lamb, A.P., and Weaver, C.S., 2017, Evidence for distributed clockwise rotation of the crust in the northwestern United States from fault geometries and focal mechanisms: Tectonics, v. 36, https://doi.org/10.1002/2016TC004223.

Bronk Ramsey, C., 2009, Bayesian analysis of radiocarbon dates: Radiocarbon, v. 51, p. 337–360.

England, P.C., and Wells, R.E., 1991, Neogene rotations and semi-continuous deformation of the Pacific Northwest continental margin: Geology, v. 19, p. 978–981, https://doi.org/10.1130/0091-7613(1991)019<0978:NRAQDO>2.3.CO;2.

Evarts, R.C., Conrey, R.M., Fleck, R.J., and Hagstrum, J.T., 2009, The Boring Volcanic Field of the Portland-Vancouver area, Oregon and Washington: Tectonically anomalous forearc volcanism in an urban setting, *in* O'Connor, J.E., Dorsey, R.J., and Madin, I.P., eds., Volcanoes to Vineyards: Geologic Field Trips through the Dynamic Landscapes of the Pacific Northwest: Geological Society of America Field Guide 15, p. 253–270.

Finn, C., 1990, Geophysical constraints on Washington convergent margin structure: Journal of Geophysical Research. Solid Earth, v. 95, p. 19,533–19,546, https://doi.org/10.1029/JB095iB12p19533.

Fitch, T.J., 1972, Plate convergence, transcurrent faults, and internal deformation adjacent to Southeast Asia and the Western Pacific: Journal of Geophysical Research, v. 77, p. 4432–4460, https://doi.org/10.1029/JB077i023p04432.

Fleck, R.J., Hagstrum, J.T., Calvert, A.T., Evarts, R.C., and Conrey, R.M., 2014, $^{40}Ar/^{39}Ar$ geochronology, paleomagnetism, and evolution of the Boring volcanic field, Oregon and Washington, USA: Geosphere, v. 10, p. 1283–1314, https://doi.org/10.1130/GES00985.1.

Freund, R., 1974, Kinematics of transform and transcurrent faults: Tectonophysics, v. 21, p. 93–134, https://doi.org/10.1016/0040-1951(74)90064-X.

Gannett, M.W., and Caldwell, R.R., 1998, Geologic framework of the Willamette lowland aquifer system, Oregon and Washington: U.S. Geological Survey Professional Paper 1424-A, 32 p., 8 plates.

Goldfinger, C., Kulm, L.D., Yeats, R.S., McNeill, L., and Hummon, C., 1997, Oblique strike-slip faulting of the central Cascadia submarine forearc: Journal of Geophysical Research. Solid Earth, v. 102, p. 8217–8243, https://doi.org/10.1029/96JB02655.

Grommé, C.S., Beck, M.E., Jr., Wells, R.E., and Engebretson, D.C., 1986, Paleomagnetism of the Tertiary Clarno Formation and its significance for the tectonic history of the Pacific Northwest: Journal of Geophysical Research, v. 91, p. 14,089–14,103, https://doi.org/10.1029/JB091iB14p14089.

Horst, A.E., Streig, A.R., and Wells, R.E., 2018, Seismic source characterization of faults in the Portland and Tualatin Basins and a paleoseismic study of the Gales Creek Fault, OR: American Geophysical Union, abstract #S41D-0561.

Horst, A.E., Streig, A.R., Wells, R.E., and Guilderson, T., 2019, Seismic source characterization of faults in the Portland and Tualatin Basins and a paleoseismic study of the Gales Creek Fault, OR: Geological Society of America Abstracts with Programs, v. 51, no. 4, https://doi.org/10.1130/abs/2019CD-329221.

Madin, I.P., 1990, Earthquake-hazard geology maps of the Portland metropolitan area, Oregon—Text and map explanation: State of Oregon, Department of Geology and Mineral Industries Open-File Report 0-90-2, 21 p., 8 pls., scale 1:24,000.

Magill, J., Cox, A., and Duncan, R., 1981, Tillamook Volcanic Series: Further Evidence for Tectonic Rotation of the Oregon Coast Range: Journal of Geophysical Research, v. 86, p. 2953–2970, https://doi.org/10.1029/JB086iB04p02953.

Magill, J.R., Wells, R.E., Simpson, R.W., and Cox, A.V., 1982, Post-12 my rotation of southwest Washington: Journal of Geophysical Research. Solid Earth, v. 87, no. B5, p. 3761–3776, https://doi.org/10.1029/JB087iB05p03761.

McCaffrey, R., Qamar, A.I., King, R.W., Wells, R.E., Ning, Z., Williams, C.A., Stevens, C.W., Vollick, J.J., and Zwick, P.C., 2007, Fault locking, block rotation, and crustal deformation in the Pacific Northwest: Geophysical Journal International, v. 169, p. 1315–1340, https://doi.org/10.1111/j.1365-246X.2007.03371.x.

McCaffrey, R., King, R.W., Payne, S.J., and Lancaster, M., 2013, Active tectonics of northwestern U.S. inferred from GPS-derived surface velocities: Journal of Geophysical Research, v. 118, https://doi.org/10.1029/2012JB009473.

McCaffrey, R., King, Robert, Wells, R.E., Lancaster, M., and Meghan Miller, M., 2016, Contemporary deformation in the Yakima fold and thrust belt estimated with GPS: Geophysical Journal International, v. 207, https://doi.org/10.1093/gji/ggw252.

McPhee, D.K., Langenheim, V.E., Wells, R.E., and Blakely, R.J., 2014, Tectonic evolution of the Tualatin Basin, northwest Oregon, as revealed by inversion of gravity data: Geosphere, v. 10, p. 264–275, https://doi.org/10.1130/GES00929.1.

Minervini, J.J., O'Connor, J.E., and Wells, R.E., 2003, Maps showing inundation depths, ice-rafted erratics, and sedimentary facies of late Pleistocene Missoula floods in the Willamette Valley, Oregon: U.S. Geological Survey Open-File Report 03-408, scale 1:250,000.

Morin, R.L., Wheeler, K.L., McPhee, D.K., Dinterman, P.A., and Watt, J.T., 2007, Principal facts of gravity data in the northern Willamette Valley and vicinity, northwestern Oregon and southwestern Washington: U.S. Geological Survey Open-File Report 2007-1058, 6 p., http://pubs.usgs.gov/of/2007/1058/.

Nelson, A.R., Johnson, S.Y., Kelsey, H.M., Wells, R.E., Sherrod, B.L., Pezzopane, S.K., Bradley, L., Koehler, R.D., and Bucknam, R.C., 2003, Late Holocene earthquakes on the Toe Jam Hill fault, Seattle fault zone, Bainbridge Island, Washington: Geological Society of America Bulletin, v. 115, no. 11, p. 1388–1403, https://doi.org/10.1130/B25262.1.

Niem, A.R., and Niem, W.A., 1985, Geologic map of the Astoria Basin, Clatsop and northernmost Tillamook Counties, northwest Oregon: Oregon Department of Geology and Mineral Industries Oil and Gas Investigations, OG-14.

Oregon Department of Geology and Mineral Industries, 2012, Western Oregon Seismic Reflection Data Imagery: Open-File Report O-12-04, 54 oversize sheets as digital files.

Oregon Water Resources Department, 2017, http://www.oregon.gov/owrd (accessed August 2017).

Personius, S.F., 1995, Late Quaternary stream incision and uplift in the forearc of the Cascadia subduction zone, western Oregon: Journal of Geophysical Research. Solid Earth, v. 100, p. 20,193–20,210, https://doi.org/10.1029/95JB01684.

Pezzopane, S.K., and Weldon, R.J., II, 1993, Tectonic role of active faulting in central Oregon: Tectonics, v. 12, p. 1140–1169, https://doi.org/10.1029/92TC02950.

Prescott, J.R. and Hutton, J.T., 1994, Cosmic ray contributions to dose rates for luminescence and ESR dating: large depths and long-term time variations: Radiation Measurements, v. 23, p. 497–500, https://doi.org/10.1016/1350-4487(94)90086-8.

Redwine, J., Klinger, R.E., Piety, L.A., Wells, R.E., Sherrod, B.L., Howe, J.C., Levinston, R., Hornsby, K., and Niem, A., 2017, Quaternary Activity on the GCF, northwest Oregon: Geological Society of America Abstracts with Programs, v. 39, no. 6, https://doi.org/10.1130/abs/2017AM-306019.

Redwine, J., Klinger, R.E., Wells, R.E., Sherrod, B.L., Mahan, S.A., Piety, L.A., Howe, J., Besana-Ostman, G., Levinson, R., Chupik, C., Cataldo, K., Nincovich, S.R., and Angster, S.J., 2019, Evidence for an active Gales Creek fault—A dynamic duo active deformation confirmation: Geological Society of America Abstracts with Programs, v. 51, no. 4, https://doi.org/10.1130/abs/2019CD-329712.

Reimer, P.J., Bard, E., Bayliss, A., Beck, J.W., Blackwell, P.G., Ramsey, C.B., Buck, C.E., Cheng, H., Edwards, R.L., Friedrich, M., and Grootes, P.M., 2013, IntCal13 and Marine13 radiocarbon age calibration curves 0–50,000 years cal BP: Radiocarbon, v. 55, p. 1869–1887, https://doi.org/10.2458/azu_js_rc.55.16947.

Schlicker, H.G., and Deacon, R.J., 1967, Engineering geology of the Tualatin Valley region, Oregon: Department of Geology and Mineral Industries Bulletin 60, 103 p.

Schuster, J.E., 2005, Geologic map of Washington state, Washington State Department of Natural Resources, scale 1:500,000.

Sevilgen, V., Stein, R.S., and Pollitz, F.F., 2012, Stress imparted by the great 2004 Sumatra earthquake shut down transforms and activated rifts up to 400 km away in the Andaman Sea: Proceedings of the National Academy of Sciences of the United States of America, v. 109, no. 38, p. 15,152–15,156, https://doi.org/10.1073/pnas.1208799109.

Sheriff, S.D., 1984, Paleomagnetic evidence for spatially distributed post-Miocene rotation of western Washington and Oregon: Tectonics, v. 3, no. 3, p. 397–408, https://doi.org/10.1029/TC003i003p00397.

Sherrod, B.L., Brocher, T.M., Weaver, C.S., Bucknam, R.C., Blakely, R.J., Kelsey, H.M., Nelson, A.R., and Haugerud, R., 2004, Holocene fault scarps near Tacoma, Washington, USA: Geology, v. 32, p. 9–12, https://doi.org/10.1130/G19914.1.

Simpson, R.W., and Cox, A., 1977, Paleomagnetic evidence for tectonic rotation of the Oregon Coast Range: Geology, v. 5, p. 585–589, https://doi.org/10.1130/0091-7613(1977)5<585:PEFTRO>2.0.CO;2.

Snavely, P.D., Jr., MacLeod, N.S., and Wagner, H.C., 1968, Tholeiitic and alkalic basalts of the Eocene Siletz River Volcanics, Oregon Coast Range: American Journal of Science, v. 266, no. 6, p. 454–481, https://doi.org/10.2475/ajs.266.6.454.

Snavely, P.D., Jr., MacLeod, N.S., Wagner, H.C., and Rau, W.W., 1976, Geologic map of the Cape Foulweather and Euchre Mountain quadrangles, Lincoln County, Oregon: U.S. Geological Survey Miscellaneous Investigations Series Map I-868, scale 1:62,500.

Stein, R.S., 1999, The role of stress transfer in earthquake occurrence: Nature, v. 402, p. 605–609, https://doi.org/10.1038/45144.

Stirling, M., Goded, T., Berryman, K., and Litchfield, N., 2013, Selection of earthquake scaling relationships for seismic-hazard analysis: Bulletin of the Seismological Society of America, v. 103, p. 2993–3011, https://doi.org/10.1785/0120130052.

Stuiver, M., and Polach, H.A., 1977, Discussion reporting of ^{14}C data: Radiocarbon, v. 19, p. 355-363.

Thomas, G.C., Crosson, R.S., Carver, D.L., and Yelin, T.S., 1996, The 25 March 1993 Scotts Mills, Oregon, earthquake and aftershock sequence; spatial distribution, focal mechanisms, and the Mount Angel fault: Bulletin of the Seismological Society of America, v. 86, no. 4, p. 925–935.

Tolan, T.L., and Reidel, S.P., 1989, Structure map of a portion of the Columbia River flood-basalt province, *in* Reidel, S.P., and Hooper, P.R., eds., Volcanism and Tectonism in the Columbia River Flood-Basalt Province: Geological Society of America Special Paper 239 [map pocket], scale 1:561,000.

U.S. Geological Survey, 2010, Quaternary fault and fold database of the United States, http://earthquake.usgs.gov/hazards/qfaults/ (accessed July 2018).

Walcott, D., 1993, Neogene tectonics and kinematics of western North America: Tectonics, v. 12, no. 2, p. 326–333, https://doi.org/10.1029/92TC02249.

Walker, G.W., MacLeod, N.S., Miller, R.J., Raines, G.L., and Connors, K.A., 2003, Spatial digital database for the geologic map of Oregon: U.S. Geological Survey Open-File Report 2003–67, https://doi.org/10.3133/ofr200367.

Walsh, K., Peterson, G.L., Beeson, M.H., Wells, R.E., Fleck, R.J., Evarts, R.C., Duvall, A., Blakely, R.J., and Burns, S., 2011, A tunnel runs through it; an inside view of the Tualatin Mountains, Oregon: U.S. Geological Survey Scientific Investigations Map 3144, 1 oversize sheet.

Wang, K., 1996, Simplified Analysis of horizontal stresses in a buttressed forearc sliver at an oblique subduction zone: Geophysical Research Letters, v. 23, p. 2021–2024, https://doi.org/10.1029/96GL02067.

Weaver, C.S., and Smith, S.W., 1983, Regional tectonic and earthquake hazard implications of a crustal fault zone in southwestern Washington: Journal of Geophysical Research, v. 88, p. 10,371–10,383, https://doi.org/10.1029/JB088iB12p10371.

Wells, R.E., and Coe, R.S., 1985, Paleomagnetism and geology of Eocene volcanic rocks of southwest Washington, implications for mechanisms of tectonic rotation: Journal of Geophysical Research. Solid Earth, v. 90, no. B2, p. 1925–1947, https://doi.org/10.1029/JB090iB02p01925.

Wells, R.E., and McCaffrey, R., 2013, Steady rotation of the Cascade arc: Geology, v. 41, p. 1027–1030, https://doi.org/10.1130/G34514.1.

Wells, R.E., and Sawlan, M.G., 2014, Preliminary geologic map of the eastern Willapa Hills, Cowlitz, Lewis, and Wahkiakum Counties, Washington, U.S. Geological Survey Open-File Report 2014-1063, two oversize sheets, scale 1:50,000.

Wells, R.E., Simpson, R.W., Bentley, R.D., Beeson, M.H., Mangan, M.T., and Wright, T.L., 1989, Correlation of Miocene flows of the Columbia River Basalt Group from the central Columbia River Plateau to the coast of Oregon and Washington, *in* Reidel, S.P., and Hooper, P.R., eds., Volcanism and Tectonism in the Columbia River Flood-Basalt Province: Geological Society of America Special Paper 239, p. 113–129, https://doi.org/10.1130/SPE239-p113.

Wells, R.E., Snavely, P.D., Jr., Macleod, N.S., Kelly, M.M., Parker, M.J., Fenton, J., and Felger, T., 1995, Geologic map of the Tillamook Highlands, northwest Oregon Coast Range—A digital database: U.S. Geological Survey Open-File Report 95-670, 2 oversize sheets, scale 1:62,500, 24 p. pamphlet, and digital database.

Wells, R.E., Weaver, C.S., and Blakely, R.J., 1998, Fore arc migration in Cascadia and its neotectonic significance: Geology, v. 26, p. 759–762, https://doi.org/10.1130/0091-7613(1998)026<0759:FAMICA>2.3.CO;2.

Wells, R.E., Jayko, A.S., Niem, A.R., Black, G., Wiley, T., Baldwin, E., Molenaar, K.M., Wheeler, K.L., DuRoss, C.B., and Givler, R.W., 2000, Geologic map and database of the Roseburg 30′ × 60′ quadrangle, Douglas and Coos Counties, Oregon: U.S. Geological Survey Open-File Report 00-0376, 2 oversize sheets, scale 1;100,000, 55 p. pamphlet, and digital database, http://geopubs.wr.usgs.gov/open-file/of00-376/.

Wells, R.E., Blakely, R.J., McPhee, D.K., and Langenheim, V.E., 2009, The Gales Creek fault accommodates large dextral offset in the Oregon forearc: Geological Society of America Abstracts with Programs, v. 41, no. 7, p. 702.

Wells, R.E., Bukry, D., Friedman, R., Pyle, D., Duncan, R., Haeussler, P., and Wooden, J., 2014, Geologic history of Siletzia, a large igneous province in the Oregon and Washington Coast Range—Correlation to the geomagnetic polarity time scale and implications for a long-lived Yellowstone hotspot: Geosphere, v. 10, no. 4, 28 p., https://doi.org/10.1130/GES01018.1.

Wells, R.E., Haugerud, R.A., Niem, A.R., Niem, W.A., Ma, L., Madin, I., and Evarts, R.C., 2018, New geologic mapping of the northwestern Willamette Valley, Oregon, and its American Viticultural Areas (AVAs)—A foundation for understanding their terroir: U.S. Geological Survey Scientific Investigations Report 2018-1044, 1 oversize sheet, https://doi.org/10.3133/ofr20181044.

Wells, R.E., Haugerud, R.A., Niem, A.R., and Niem, W.A., Ma, Lina, Evarts, R.C., O'Connor, J.E., Madin, I.P., Sherrod, D.R., Beeson, M.H., Tolan, T.L., Wheeler, K.L., Hanson, W.B., and Sawlan, M.G., 2019, Geologic map of the greater Portland metropolitan area and surrounding region, Oregon and Washington: U.S. Geological Survey Scientific Investigations Map 3443, 1 oversize sheet, pamphlet, and geodatabase, scale 1:63,360.

Werner, K.S., Graven, E.P., Berkman, T.A., and Parker, M.J., 1991, Direction of maximum horizontal compression in western Oregon determined by borehole breakouts: Tectonics, v. 10, p. 948–958, https://doi.org/10.1029/90TC01288.

Wheeler, K.L., Wells, R.E., Minervini, J.M., and Block, J.L., 2009, Geologic map of the Carlton quadrangle, Yamhill County, Oregon: U.S. Geological Survey Open-File Report 2009-1172, 1 oversize sheet, scale 1:24,000 and database.

Wilson, D.C., 1997, Post-middle Miocene geologic history of the Tualatin Basin, Oregon, with hydrologic implications [unpublished Ph.D. dissertation]: Portland, Oregon, Portland State University, 321 p.

Wilson, D.C., 1998, Post-middle Miocene geologic evolution of the Tualatin Basin, Oregon: Oregon Geology, v. 60, no. 5, p. 99–116.

Wilson, D.S., 1993, Confidence intervals for motion and deformation of the Juan de Fuca plate: Journal of Geophysical Research. Solid Earth, v. 98, no. B9, p. 16,053–16,071, https://doi.org/10.1029/93JB01227.

Yeats, R.S., Graven, E.P., Werner, K.S., Goldfinger, C., and Popowski, T.A., 1996, Tectonics of the Willamette Valley, Oregon, *in* Rogers, A.M., Walsh, T.J., Kockelman, W.J., and Priest, G.R., eds., Assessing Earthquake Hazards and Reducing Risk in the Pacific Northwest: U.S. Geological Survey Professional Paper 1560, p. 183–222.